TÉCNICO LISBOA

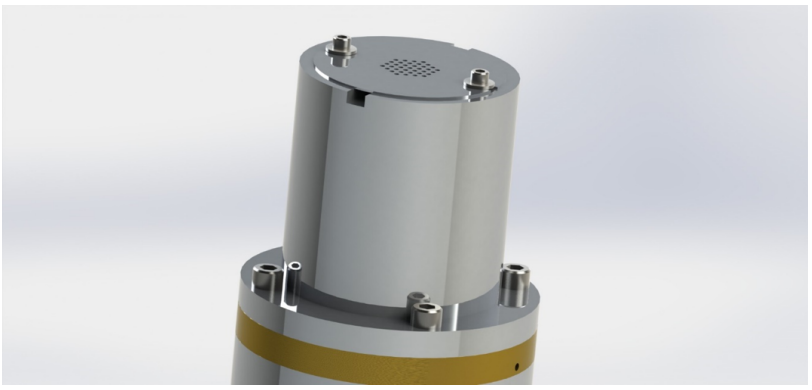

Helmholtz resonator with multi-perforated plate

Diogo Filipe Alves Cabral

Thesis to obtain the Master of Science Degree in

Mechanical Engineering

Supervisors: Prof. Edgar Caetano Fernandes
Prof. Aires José Pinto dos Santos

Examination Committee

Chairperson: Prof. Viriato Sérgio de Almeida Semião
Supervisor: Prof. Edgar Caetano Fernandes
Member of the Committee: Prof. Fernando José Parracho Lau

November 2016

Acknowledgments

I would like to thank my parents for giving me the possibility to achieve this degree, to professors Edgar Fernandes and Aires Santos for all the insight and guidance in the development of this work and to my lab friends Miguel Machado and Miguel Ferreira for helping me solve technical difficulties and for the coffee breaks.

Resumo

Pretende-se com este estudo modelar a acústica de ressonadores de Helmholtz quando uma chapa perfurada é colocada no topo. A geometria típica de um ressonador de Helmholtz - que consiste essencialmente numa cavidade de ar ligada a uma pequena abertura - pode ser encontrado em diversas aplicações, como por exemplo um carro com uma janela aberta, tectos falsos, garrafas, queimadores industriais presentes em fornalhas e aquecedores, etc. Devido à presença da chapa metálica perfurada no topo da abertura do ressonador, o comportamento acústico será diferente, pelo que é necessário uma extensão da teoria acústica dos ressonadores de Helmholtz. No modelo matemático, a chapa metálica no topo dos ressonadores comporta-se como uma impedância adicional no sistema. Foi observado que a frequência de ressonância, quando a chapa é introduzida, é reduzida de acordo com as características da chapa, como a porosidade e o rácio de perfuração. Os diâmetros das aberturas variam entre $7 - 25.4$ mm, e os volumes das cavidades variam entre $90 - 250 * 10^{-6}$ m^3. As chapas têm uma espessura de 0.5 mm com diferentes configurações de furos, com diâmetros de furo que variam entre $0.6 - 6$ mm e espaçamento entre furos de $1.5 - 5$ mm. Os resultados demonstram que o modelo matemático prevê os resultados experimentais.

Palavras-chave: Helmholtz, ressonador, perfurações, chapas, acústica

Abstract

The present work focuses on evaluating the acoustic behavior of a Helmholtz resonator when a thin metal plate, with small perforations, is introduced on the top. The basic geometry of the Helmholtz resonator, which consists of a volume of air connected to a small neck, can be found in many different applications, examples are such as a car with an open window, fake ceilings, water bottles, industrial burners present in furnaces and heaters, etc. Due to the presence of a plate with small perforations on the neck, an extension to the acoustic theory concerning Helmholtz resonators is proposed. In the mathematical model, the plate on the top of the resonator acts as an additional impedance in the system. It was observed that the resonance frequency, when the plate is introduced, decreases according to the characteristics of the plate, such as the porosity and perforation ratio. The diameter of the necks ranged from $7 - 25.4$ mm, and the volume of the cavity of the resonators ranged from $90 - 250 * 10^{-6}$ m^3. The plates have a thickness of 0.5 mm with varying geometry configurations for the perforated holes, with hole diameters ranging from $0.6 - 6$ mm and hole spacing from $1.5 - 5$ mm. The results demonstrate that the mathematical model predicts the experimental results.

Keywords: Helmholtz, resonator, perforated, plates, acoustics

Contents

List of Tables

List of Figures

Nomenclature

Acronyms

MPP	Multi-perforated plate.
SPL	Sound pressure level.

Greek symbols

μ	Absolute viscosity.
α_w	Absorption coefficient at the wall.
ω	Angular frequency.
α_{wk}	Component of the absorption coefficient at the wall due to thermal conduction.
$\alpha_{w\eta}$	Component of the absorption coefficient at the wall due to viscous dissipation.
ω_a	Damped angular frequency.
δ	Damping ratio.
ξ	Displacement coordinate.
δ_c	End-correction term defined by Ingard and Ising.
ρ_0	Equilibrium density.
γ	Heat capacity ratio.
ν	Kinematic viscosity.
ϕ	Perforation ratio.
σ	Porosity.
σ_M	Porosity defined by Muttalip.
ω_0	Resonant angular frequency.
λ	Wavelength.

Roman symbols

P_c Acoustic pressure amplitude within the cavity.

R_r Acoustic radiation losses.

S_f Area of a single perforation.

$S(x)$ Area variation of the resonator along x

A_b Base area of the volume.

u_c Critical value of u_0.

l' Corrected neck length.

b Damping term.

d_p Diameter of a single perforation.

P External driving pressure amplitude of the incident wave.

$F(t)$ External perturbation variable in time.

l_v Form factor.

h Height of the resonator from the bottom to the neck.

Z_{HR} Impedance of the Helmholtz resonator.

Z_{MPP} Impedance of the multi-perforated plate.

m Mass of air in the neck.

R_m Molar gas constant.

n Number of perforations in a plate.

l_{01} Outer neck end-correction.

l_{02} Outer neck end-correction.

Pr Prandtl number.

p Pressure within the cavity.

S_a Polygon area.

a Radius of the neck.

X Reactance term of the impedance.

R Resistance term of the impedance.

f_0 Resonant frequency.

S	Resonator neck area.
l	Resonator neck length.
V	Resonator volume.
Sh	Shear number.
c	Speed of sound.
Z_0	Specific acoustic impedance.
k	Stiffness constant.
Sr	Strouhal number.
T	Temperature of air.
R_w	Thermoviscous losses.
t_p	Thickness of the plate.
t	Time.
$V(x)$	Total volume of the resonator at x.
u_0	Velocity amplitude in the orifice.
C_{vc}	Vena-contracta factor.
V_{01}	Volume of the hypothetical elongation of the neck due to the motion of gas.
V_n	Volume of the neck.
k_n	Wavenumber.

Chapter 1

Introduction

1.1 Context

In this introductory section a brief description about the Helmholtz resonator and applications are presented for context purposes. The Helmholtz resonator consists essentially of a cavity connected to an outer opening. These resonators find most applications in acoustics to amplify or attenuate sound waves, namely in musical instruments to amplify certain frequencies to produce a desired tone and internal combustion engines to attenuate the high noise levels produced by the combustion engine (ICEs)[1]. However they are also present in different scenarios, such as a car with an open window where the air inside the car acts as the cavity in the Helmholtz resonator analog, fake ceilings where the end goal is attenuate sound noise produced inside the room by perforating small openings backed with a large cavity in the ceilings, and the most common example is an empty bottle where the air inside the neck vibrates when you blow air across the top, generating the typical low sound. The burners presented in this work have the same configuration as the Helmholtz resonator, as shown in figures 1.1 and 1.2. These burners have this design because the initial concept of a burner was essentially a pre-mixing cavity for the fuel and air followed by a small exit for the flame, which ended having the geometry of a Helmholtz resonator.

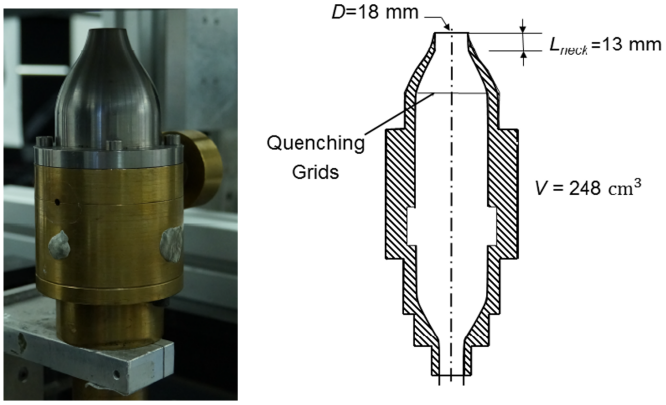

Figure 1.1: Helmholtz burner schematics. Adapted from [2]

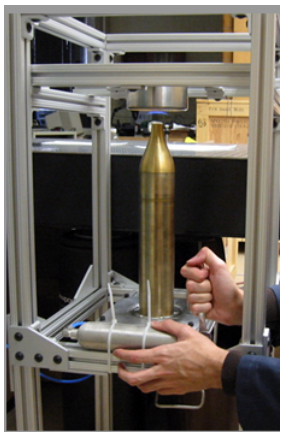

Figure 1.2: Helmholtz burner, Adapted from http://afl.mcgill.ca/AFL-Research.html

These burners are usually present in industrial furnaces, domestic stoves (single or multiple openings), heaters, etc. As shown by Cintra and Fernandes [2], when the burners are at burning conditions - where the air and fuel are introduced from the lower part into the cavity - they can produce different types of flames as shown in figure 1.3, where the exit of the burner was placed at a certain distance from a flat wall:

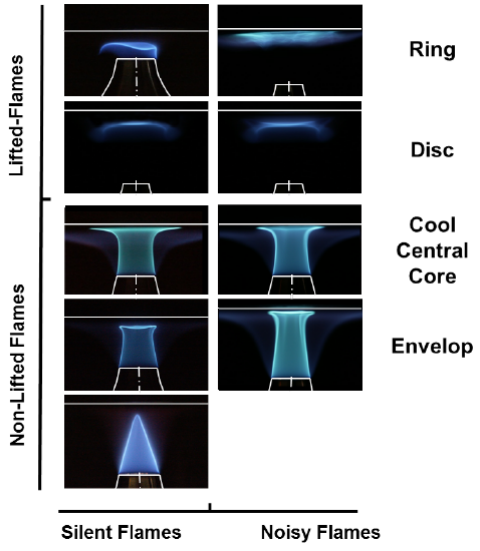

Figure 1.3: Helmholtz burner flame types. Adapted from [2]

Thermoacoustic instabilities occur in these burners where some flames are silent and other flames are noisy. There are a few different ways to prevent such instabilities, namely by either changing the burning conditions (air-fuel ratio, Reynolds number, etc.) or by changing the geometry of the burner (which changes the acoustics). However the focus of this work as stated in the abstract is to study the acoustics of Helmholtz burners with a perforated plate on top to produce very small flames, as shown by figure 1.4, where it is presented a burner consisting of a cylindrical mixing cavity with an opening with small holes.

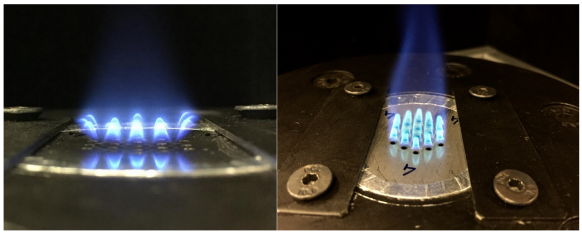

Figure 1.4: Two examples of very small flames ($\approx 2mm$)

These flames also produce thermoacoustic instabilities, however for this case of very small flames, the instability regimes have not been studied as deeply as in the previous case. Finally in order to create the small flames on Helmholtz burners, a thin metal plate is introduced at the top of the burner as shown in figure 1.5. However by introducing the metal plate on the top, the acoustics of the system will change according to the characteristics of the plate, which is the main objective of this work.

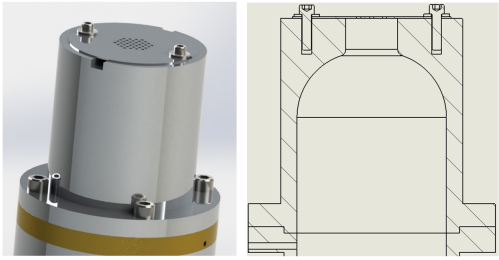

Figure 1.5: Helmholtz resonator with multi-perforated plate

1.2 Objectives

The ultimate objective of this work is to predict the unstable frequencies of a Helmholtz resonator when a multi-perforated plate (MPP) is inserted on the top of the neck (figure 1.5) and to develop a theoretical model that matches experimental data.

1.3 Thesis Outline

Initially a literature review about the current theory and variants regarding the Helmholtz resonator is conducted. Then a theoretical model is explained with detail regarding the influence of the metal plate on top of the resonator. After a brief explanation of the experimental installation used for all the tests, data acquisition is presented followed by a discussion of the results which are compared to the theoretical model.

Chapter 2

Literature review

This study focuses on the Helmholtz resonator type of burners, as mentioned previously. These types of burners follow an acoustic model known as the Helmholtz resonator, and research in the literature was conducted as a starting point for this work.

2.1 What is a Helmholtz resonator?

A Helmholtz resonator, originally created and developed by Hermann von Helmholtz in the 1850's, is a cavity with a volume *V* filled with a gas (usually air) connected to a neck of length *l* and area *S* as shown in figure 2.1.

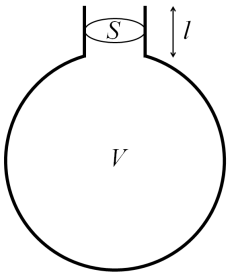

Figure 2.1: Helmholtz Resonator

If the mass of air in the neck is excited by an external acoustic wave or flow, it will vibrate at a certain frequency, generating a specific sound wave response. Helmholtz resonators have been used for more than 100 years in many different applications, but mainly to effectively reduce the high wavelength sounds, i.e. attenuate the narrow-band low-frequency noise. The classic lumped theory which is commonly found in the literature approximates a Helmholtz resonator to a mass-spring-damper system to be able to predict the acoustics, and yields the expressions for the resonator frequency and the transmission loss ([3],[4],[5],[6]). A number of studies ([7],[8],[9],[10]) have also developed a one-dimensional analytical approach to investigate the wave attenuation properties. In many cases the approximation of a one-dimensional model is not fully accurate due to complex geometries or the presence of non-

linear phenomena, and to account for the non-planar wave propagation in both the neck and the cavity of the resonator, multi-dimensional models have also been employed to model the sound attenuation in Helmholtz resonators with different shapes due to practical reasons, such as with circular concentric cavity [10], circular asymmetric cavity [11], extended neck into the resonator cavity [12], and with absorbing material present in the cavity [13].

Over the years these types of resonators have been useful in a number of applications, for both attenuation and amplification of sound waves, especially in engineering and acoustics. Since the development of technology demanded the use of these resonators due to noise regulations the Helmholtz resonator became a subject of extensive research to improve its characteristics. Selamet and Lee [12] studied the effect of geometry on the resonance frequency and transmission loss of concentric circular Helmholtz resonators. Selamet et al. [13] developed a 2D analytical solution to investigate the effect of density and thickness of the fibrous material in the cavity on the resonance frequency and transmission loss of circular Helmholtz resonators lined with absorbent. Tang [14] investigated experimentally and theoretically the Helmholtz resonators with tapered necks. Wan and Soedel [15] derived an expression for the resonance frequencies of two degree-of-freedom Helmholtz resonator using a lumped model. De Bedout et al. [16] proposed a tunable Helmholtz resonator with a feedback system so that the resonator can be tuned to a range of resonant frequencies. Griffin et al. [17] developed an analytical model for a single, coupled resonator system mounted on a one-dimensional duct.

2.2 The Helmholtz Resonator

2.2.1 Classic model

Consider the system based on a volume *V* with a neck of length *l* and area *S*, as shown in Figure 2.2.

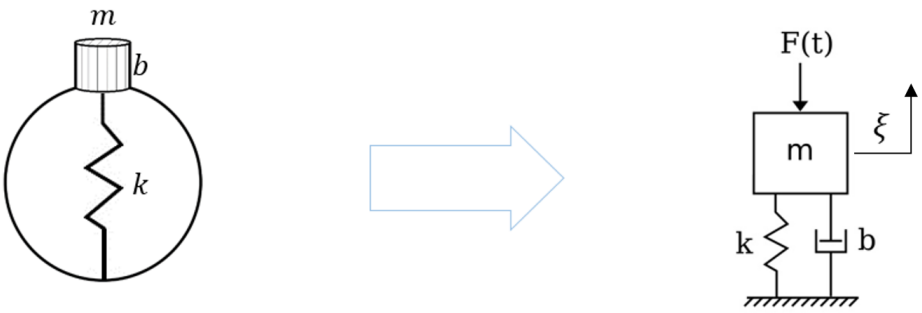

Figure 2.2: Helmholtz Resonator Model

For certain frequencies where the acoustic wave that is acting on the system has a larger wavelength λ than any length of the structure, namely $\lambda \gg l$, $\lambda \gg V^{1/3}$ and $\lambda \gg S^{1/2}$, the Helmholtz resonator can be modeled as a mechanical lumped acoustic system i.e. a one degree-of-freedom mass-spring system with damping.

The volume *V* acts has a spring because it is confined in the cavity and can only contract and

expand due to the motion of the mass *m* above it, behaving as a locally closed system. When the first perturbation acts on the mass in the neck, it will move down by a certain displacement ξ. This causes a pressure rise in the volume, pushing the mass upward. When this mass is at a certain level above the neck the pressure inside the volume decreases (because the volume increased) to the point where the net force acting on the mass can change it's momentum to the opposite direction, and so it pushes the mass back down again, repeating the cycle. In the general time spectrum where the Helmholtz resonator is actuated with an incident cyclic perturbation, the mass will vibrate under a certain frequency and phase. The damper takes into account the losses in the whole system (mainly in the neck).

The displacement ξ in an one degree-of-freedom mass-spring system with damping is determined by the solution of an ordinary second order differential equation:

$$m\frac{d^2\xi}{dt^2} + b\frac{d\xi}{dt} + k\xi = SPe^{iwt} \tag{2.1}$$

where P represents the pressure amplitude of the sound wave at time t with an angular velocity ω. It is well known that the resonant frequency of this system, for $b = 0$, is:

$$\omega_0 = \sqrt{\frac{k}{m}} \tag{2.2}$$

Since this system has damping, $b \neq 0$, the real (i.e. damped) resonant frequency is given by:

$$\omega_a \quad = \quad \omega_0\sqrt{1-\delta^2} \tag{2.3}$$

where $\delta = \frac{b}{\sqrt{2}m\omega_0}$ is the damping ratio.

In the following section the mathematical formulation of each term of the equation is described. It was verified that an end correction was necessary to be made in the length l of the neck for the mass m to take into account the geometry of the edge and the influence on motion of air on the surroundings. The effective mass is [5]:

$$m = \rho_0 S l' \tag{2.4}$$

where [5]:

$$l' \quad = \quad l + 1.7a \; (outer \; end \; flanged) \tag{2.5}$$

$$l' \quad = \quad l + 1.4a \; (outer \; end \; unflanged) \tag{2.6}$$

with ρ_0 being the equilibrium density, a being the radius of the neck with area S.

Different corrections for the length of the neck are also found in the literature. Ingard [4] states that the total correction of the neck length has two contribuitions: one inner end-correction δ_i present on the

volume side of the neck and one outer end-correction δ_0 present in the outer side of the neck, given by [4]:

$$\delta_0 = \frac{8a}{3\pi} \tag{2.7}$$

$$\delta_i = \delta_0 \left(1 - 1.25\frac{S}{A_b}\right) \tag{2.8}$$

where A_b is the area of the volume base.

The pressure increase by a displacement $d\xi$ is given by [5]:

$$dp = -\frac{\rho_0 c^2 S}{V} d\xi \tag{2.9}$$

where c represents the speed of sound, which for a perfect gas, is $c = \sqrt{\gamma R_m T}$, T being the temperature of air, with a heat capacity ratio for air $\gamma \approx 1.4$.

Knowing the relation $dF = Sdp = -kd\xi$ then the effective stiffness is:

$$k = \frac{\rho_0 S^2 c^2}{V} \tag{2.10}$$

Finally to formulate the damper b some assumptions must be made. The total damping of the system comes from mainly two contributions: acoustic radiation and thermoviscous losses in the neck.

$$b = R_r + R_w \tag{2.11}$$

Assuming that the moving fluid in the neck radiates sound into the surrounding medium in the same manner as an open-ended pipe, the acoustic radiation resistance [5]:

$$R_r = \frac{\rho_0 c k_n^2 S^2}{2\pi} \; (outer\ end\ flanged) \tag{2.12}$$

$$R_r = \frac{\rho_0 c k_n^2 S^2}{4\pi} \; (outer\ end\ unflanged) \tag{2.13}$$

The thermoviscous losses term is obtained by calculating the wall losses, which gives [5]:

$$R_w = 2mc\alpha_w \tag{2.14}$$

with α_w being the absorption coefficient with two contribuitions: viscous dissipation in the acoustic boundary layer and thermal conduction through the wall, given by [5]:

$$\alpha_w = \alpha_{w\mu} + \alpha_{wk} = \frac{1}{ac}\left(\frac{\mu\omega}{2\rho_0}\right)^{1/2}\left(1 + \frac{\gamma - 1}{\sqrt{Pr}}\right) \tag{2.15}$$

where μ is the absolute viscosity and *Pr* the Prandtl number. Assuming that the response to this type of solicitation is also harmonic then $\xi(t) = \xi_0 e^{i\omega t}$. Using equation (2.1) and knowing that $\frac{d^2\xi}{dt^2} = -\omega^2 \xi_0 e^{i\omega t}$

gives:

$$(-m\omega^2 + k + i\omega b)\xi_0 e^{i\omega t} = SPe^{i\omega t} \tag{2.16}$$

By solving the previous equation (2.16), the maximum of the displacement is:

$$\xi_0 = \frac{1}{i\omega}\frac{SP}{b + i(\omega m - \frac{k}{\omega})} \tag{2.17}$$

Using equations (2.4), (2.10) and (2.11) to equation (2.1), the equation for the Helmholtz resonator system displacement is:

$$\rho_0 S\left(l + (1.7\ or\ 1.4)a\right)\frac{d^2\xi}{dt^2} + \left(\frac{\rho_0 c k_n^2 S^2}{(2\ or\ 4)\pi} + \frac{2m}{a}\left(\frac{\mu\omega}{2\rho_0}\right)^{1/2}\left(1 + \frac{\gamma - 1}{\sqrt{Pr}}\right)\right)\frac{d\xi}{dt} + \frac{\rho_0 S^2 c^2}{V}\xi = SPe^{iwt} \tag{2.18}$$

The solution to equation (2.18) is:

$$\xi_0 = \frac{1}{i\omega}\frac{SP}{\left(\frac{\rho_0 c k_n^2 S^2}{(2\ or\ 4)\pi} + \frac{2m}{a}\left(\frac{\mu\omega}{2\rho_0}\right)^{1/2}\left(1 + \frac{\gamma-1}{\sqrt{Pr}}\right)\right) + i\left(\omega(\rho_0 S l') - \frac{\rho_0 S^2 c^2}{V\omega}\right)} \tag{2.19}$$

The formula for the pressure fluctuations inside the volume is given by [5]:

$$P_c = \frac{\rho_0 c^2 S}{V}\xi_0 \tag{2.20}$$

With equations (2.20) and (2.17) it is possible to obtain the transfer function - ratio of the acoustic pressure amplitude within the cavity to the external driving pressure amplitude of the incident wave - which is:

$$\frac{P_{in}}{P} = \left(\frac{\rho_0 c^2 S^2}{i\omega V}\right)\left[b + i\left(\omega m - \frac{k}{\omega}\right)\right]^{-1} \tag{2.21}$$

Expanding the terms of equation (2.21) gives:

$$\frac{P_{in}}{P} = \left(\frac{\rho_0 c^2 S^2}{i\omega V}\right)\left[\left(\frac{\rho_0 c k_n^2 S^2}{(2or4)\pi} + \frac{2m}{a}\left(\frac{\mu\omega}{2\rho_0}\right)^{1/2}\left(1 + \frac{\gamma - 1}{\sqrt{Pr}}\right)\right) + i\left(\omega(\rho_0 S l') - \frac{\rho_0 S^2 c^2}{V\omega}\right)\right]^{-1} \tag{2.22}$$

2.2.2 Linear Impedance

A mechanical impedance for the Helmholtz resonator can be deduced and has the following form [5]:

$$Z_{HR} = b + i\left(\omega m - \frac{k}{\omega}\right) = R + iX \tag{2.23}$$

where *R* is the real part and represents the resistance and *X* is the imaginary part and represents the reactance of the system. It is the denominator of the second fraction of equation (2.17). The resonant frequency is achieved when the reactance goes to zero and according to equation (2.23) and knowing $f_0 = \omega_0/2\pi$ gives:

$$\omega_0 m - \frac{k}{\omega_0} = 0 \quad => \quad f_0 = \frac{c}{2\pi}\sqrt{\frac{S}{Vl'}} \tag{2.24}$$

Ingard and Ising [18] have shown through experiments the variation of the impedance Z for a single orifice, which can be analogous to the neck of the resonator, as depicted in figure 2.3. This research is presented here to show how the impedance varies according to the intensity of the perturbation. The results indicate that in the linear regime the resistance and reactance, for an orifice, are $R = (8\mu\rho_0\omega)^{1/2}(1 + t_p/d_p)$ and $X = \omega\rho_0(t_p + \delta_c)$ respectively, where t_p is the thickness of the orifice, d_p the diameter and δ_c is an end-correction term. The linear regime is defined by the condition $u_0 < u_c$ where u_0 is the velocity amplitude in the orifice and $u_c = (1 + t_p/d_p)(8\omega\mu/\rho_0)^{1/2}$ is a critical value.

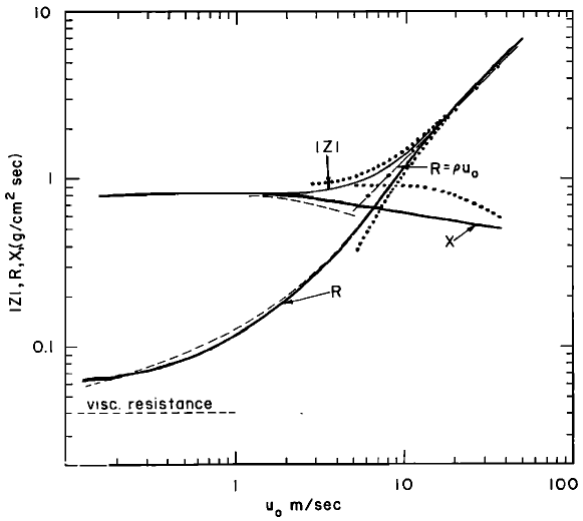

Figure 2.3: Variation of impedance R, X and $|Z|$ for an orifice dependent on the velocity in the neck u_0. (-) frequency-response measurements, (·) hot-wire measurements [18]

2.2.3 Transition regime and Non-linear Impedance

A practical description of the transitional behavior is provided between the linear and strongly non-linear regimes, and although the latter is a large influence on the acoustic behavior, the transition from one to another has not been a focus of interest so far.

The non-linear regime, according to Ingard and Ising [18] and shown in figure 2.3, occurs for $u_0 \gg u_c$

and results show that this condition is satisfied for $u_0 \gg 25u_c = 25(1 + t_p/d_p)(8\omega\mu/\rho_0)^{1/2}$. At high velocity amplitudes in the orifice the resistance is $R = \rho u_0$ (as predicted experimentally and shown in figure 2.3) and the reactance X approaches a value approximatelly one-half the linear value. The increase in orifice resistance is caused by the kinetic energy dissipation in the form of jets, however the decrease in reactance is generally attributed to the decrease in the inertia of the fluid oscillating in the exit region; the latter is related to the formation of the jet. A schematic description of a single hole is described in the following figure 2.4.

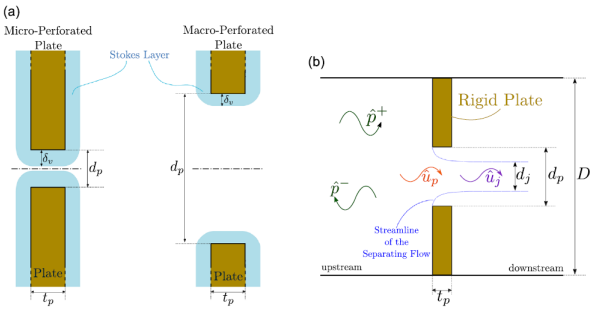

Difference between micro and macro-perforated plates.

Quasi-steady flow under the influence of high level acoustic excitation.

Figure 2.4: Orifice geometry (a) and the quasi-steady acoustic flow (b) with orifice diameter d_p, plate thickness t_p, channel diameter D, Stokes layer thickness δ_v, (complex) acoustic pressure p and (complex) acoustic particle velocity $\widehat{u}$ where the subscripts p and j imply perforation and jet flow respectively (a) Difference between micro and macro-perforated plates. (b) Quasi-steady flow under the influence of high level acoustic excitation [19].

In the linear case the absorption of the acoustic energy produced by the harmonic perturbation takes place in the Stokes layers shown in figure (2.4). The layers are formed due to the presence of the wall. The thickness of the oscillating Stokes layer is $\delta_v = \sqrt{\mu/\omega\rho_0}$ and the Stokes layer thickness, relative to the perforation diameter d_p, is referred in the literature as the Shear number given by [19]:

$$Sh = \frac{d_p}{2\delta_v} = d_p\sqrt{\frac{\omega\rho_0}{4\mu}} \tag{2.25}$$

When the excitation amplitude is larger than a critical value, which means entering the non-linear regime, vortices start forming at the sharp corners of the perforation, and they may remain in the vicinity of the hole depending on the SPL (Sound pressure level). The criteria for these vortices to start forming is based on the oscillating velocity and are quantified by the Strouhal number, which is calculated as [19]:

$$Sr = \frac{\omega d_p}{|\widehat{u}_p|} \tag{2.26}$$

where $|\widehat{u}_p|$ is the cross-sectional surface averaged acoustic velocity amplitude at the orifice.

Muttalip et al. [19] observed that the amplitude of the perturbation causes different behaviors on the boundary layer thickness depending on the regime which can be characterized in two non-dimensional numbers, the Strouhal and the Shear numbers, and as a result it can change the complex impedance of

the resonator. If the thickness of this boundary layer is in the order of magnitude of the diameter, then the Shear number is expected to be in the order of unity. For $Sr \gg 1$, the particle displacement $\widehat{u}_p/\omega$ is smaller than the orifice diameter d_p and vortices are unlikely to be observed, which is the case for the linear regime. In the opposite limit, $Sr \ll 1$, the particle displacement in the vicinity of the orifice is so large that vortices are blown away by the acoustic flow, which can be described for this strongly non-linear regime, vortex shedding dominates the absorption of the acoustic energy as a free jet. In between these two limiting cases, i.e. $Sr = O(1)$, vortices form at the edges of the perforations but they remain local and attached to the edges. To better illustrate the vortex shedding dynamics, Roche et al. [20] studied these vortexes as shown in figures 2.5, 2.6, and 2.7 and present different cases according to the SPL and frequency:

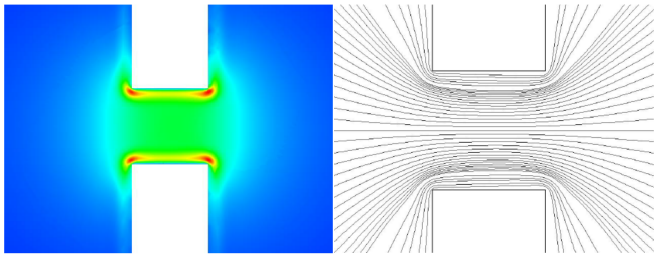

Figure 2.5: Instantaneous velocity vector (left) and streamline pattern (right). SPL = 80 dB (low SPL) at eigenfrequency 1.7 kHz [20]

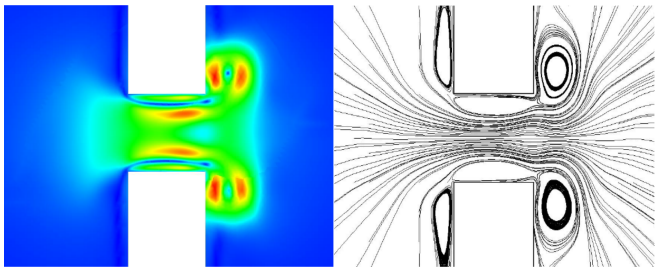

Figure 2.6: Instantaneous velocity vector (left) and streamline pattern (right). SPL = 130 dB (moderate SPL) at eigenfrequency 1.7 kHz [20]

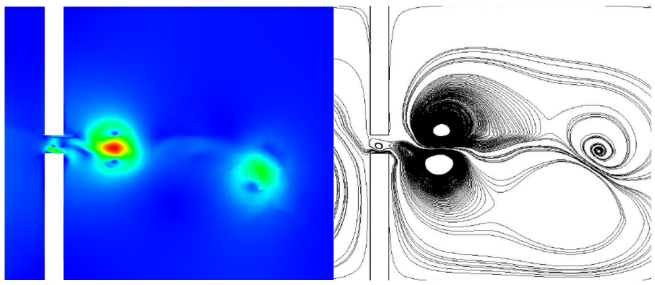

Figure 2.7: Instantaneous velocity vector (left) and streamline pattern (right). SPL = 150 dB (high SPL) at eigenfrequency 1.7 kHz [20]

Note that $u_p \propto$ SPL because the amplitude of the soundwave is larger as SPL increases. In figure 2.5 - at low SPL levels - it is observed that the flow remains laminar in the hole ($Sr \gg 1$) revealing

no vortex shedding. Figure 2.6 shows the intermediate case where a moderate SPL causes vortex shedding but they keep attached to the hole ($Sr = O(1)$). In the limiting case shown in figure 2.7, the SPL is high enough to cause vortex shedding ($Sr \ll 1$). The empirical expressions are presented to take into account non-linear effects, specifically the changes in the resistive and reactance part of the acoustic impedance of a resonator with sharp square edges [19]:

$$R_{total} = R_{linear} + \frac{F_c(Sr, Sh)|u_p|\rho_0}{2C_{vc}^2\sigma_M} \tag{2.27}$$

$$X_{total} = X_{linear} + \frac{G_c(Sr, Sh)\omega\rho_0 d_p}{2\sigma_M} \tag{2.28}$$

where $\sigma_M = (d_p/D)^2$ is the porosity defined by Muttalip [19], C_{vc} is the vena-contracta factor, which takes into account the location of the maximum velocity through the orifice caused by a flow through an orifice. Functions F_c and G_c area empirical functions for the non-linear components obtained from experiments, which will be presented next.

In order to quantify the non-linear effects, Muttalip et al. [19] performed several experiments with different sharp edged holes changing the value of Sr, as shown in the following figures.

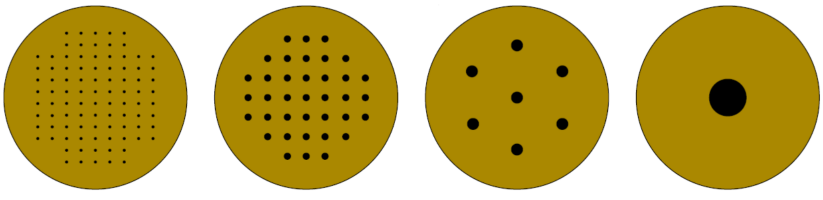

Sample	d_p (mm)	t_p (mm)	σ_M(%)	C_{vc}
Sample A	0.3	1.0	0.77	0.70
Sample B	0.8	1.6	0.74	0.70
Sample C	1.6	1.6	0.72	0.70
Sample D	4.2	4.0	0.71	0.70

Figure 2.8: Macro and micro sized holes. $\sigma_M = (d_p/D)^2$ is the porosity and C_{vc} the vena-contracta factor [19].

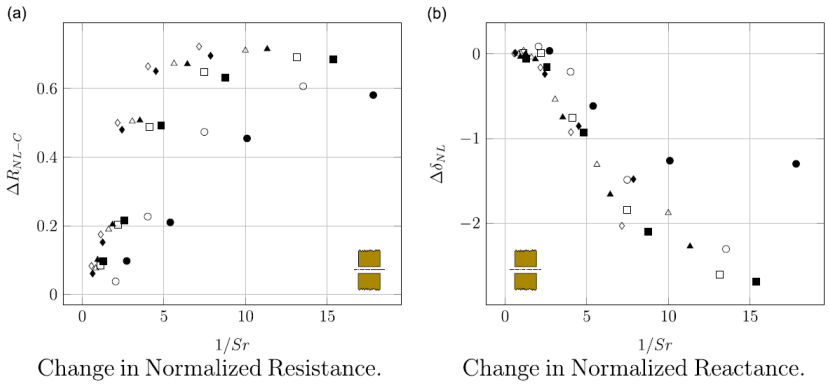

Figure 2.9: The effect of Sh number for Sample A: • Sh = 0,75; ○ Sh = 0,86; ■ Sh = 1,05; □ Sh = 1,14; ▲ Sh = 1,22; △ Sh = 1,29; ♦ Sh = 1,43; ◊ Sh = 1,49. (a) Change in normalized resistance. (b) Change in normalized reactance [19].

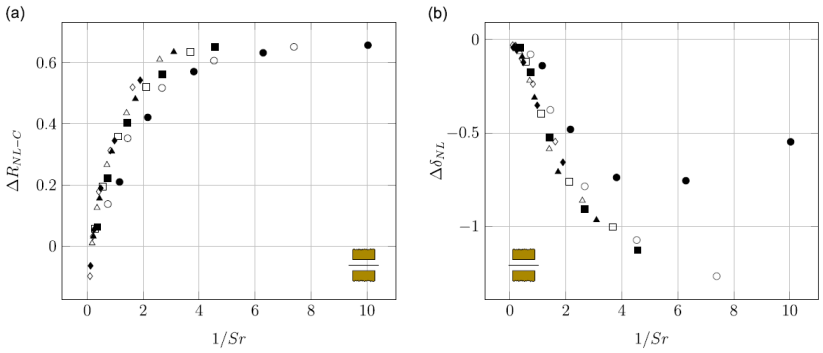

Change in Normalized Resistance. Change in Normalized Reactance.

Figure 2.10: The effect of Sh number for Sample B: • Sh = 1,99; ○ Sh = 2,29; ■ Sh = 2,81; □ Sh = 3,04; ▲ Sh = 3,25; △ Sh = 3,44; ♦ Sh = 3,81; ◊ Sh = 3,98. (a) Change in normalized resistance. (b) Change in normalized reactance [19].

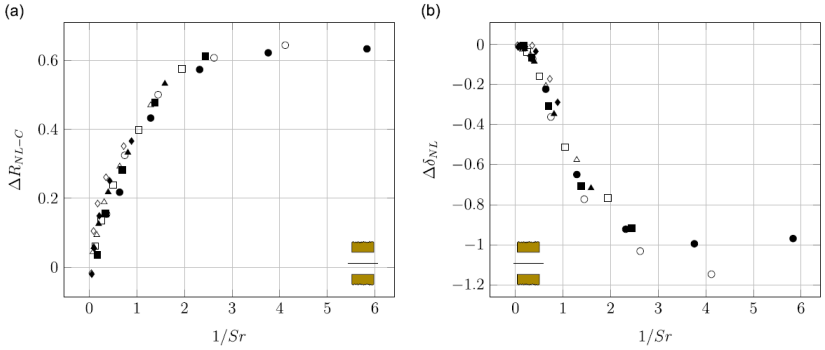

Change in Normalized Resistance. Change in Normalized Reactance.

Figure 2.11: The effect of Sh number for Sample C: • Sh = 3,98; ○ Sh = 4,59; ■ Sh = 5,62; □ Sh = 6,07; ▲ Sh = 6,49; △ Sh = 6,88; ♦ Sh = 7,61; ◊ Sh = 3,98. (a) Change in normalized resistance. (b) Change in normalized reactance [19].

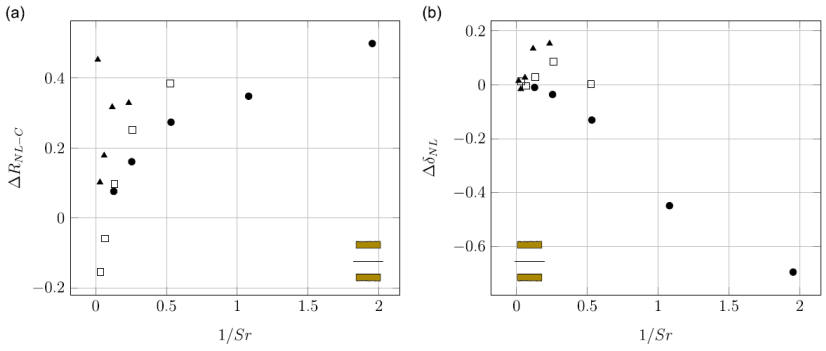

Change in Normalized Resistance. Change in Normalized Reactance.

Figure 2.12: The effect of Sh number for Sample D: • Sh = 3,98; □ Sh = 6,07; ▲ Sh = 6,49; (a) Change in normalized resistance. (b) Change in normalized reactance [19].

ΔR_{NL} and $\Delta \delta_{NL}$ represent the non-dimensional resistance and reactance change due to non-

linearity, respectively [19]:

$$\Delta R_{NL} = \frac{(R(Z_{NL}) - R(Z_L))\sigma}{|\widehat{u}_p|\rho_0} * 2C_{vc}^2 \tag{2.29}$$

$$\Delta \delta_{NL} = \frac{(X(Z_{NL}) - X(Z_L))\sigma}{\omega \rho_0 d_p/2} \tag{2.30}$$

The non-linear effects expressed by the Strouhal number Sr cannot be ignored for $Sh = O(1)$. The most prominent result of the study is that in the transition regime, the non-linear corrections both for resistance and reactance depend mainly on Sr and Sh. The dependance on Sh becomes negligible for values of $Sh > 3$. In Figure 2.9 where the sample A is tested, it is seen that for $Sh = O(1)$ the effect of the Shear number cannot be ignored. As the shear number increases this dependence vanishes due to non-linearities. The non-linear contribution to the resistance is proportional to the square of the acoustic amplitude (and Reynolds number) and the increase in resistance can be up to 60% at high amplitude due to non-linear effects. For the reactance, conclusions are not straightforward. The value of $\Delta\delta_{NL}$ approaches zero as Sr increases, regardless of the Sh value, but for $Sr \ll 1$ there is no clear trend. For the samples B and C (figures 2.10 and figure 2.11), conclusions are similar, i.e as the shear number Sh increases the deviations ΔR_{NL} and $\Delta\delta_{NL}$ become smaller.

From the experimental data it is now possible to obtain the correlations of the functions F_c and G_c stated previously and have the following form [19]:

$$F_c(Sr, Sh) = \frac{1}{1 + 2Sr[1 + 0,06exp(3,74/Sh)]} \tag{2.31}$$

$$G_c(Sr, Sh) = \begin{cases} 0,20 - \frac{0,50}{Sr}\left(1 - \frac{0,42}{Sh^2}\right) + \frac{0,05}{Sr^2}\left(1 - \frac{0,68}{Sh^2}\right), & \text{if } Sr \leq 1 \\ -0,05\left[\frac{1}{Sr}\left(1 - \frac{1}{Sh}\right)\right] - 0,6\left[\frac{1}{Sr}\left(1 - \frac{1}{Sh}\right)\right]^2, & \text{otherwise} \end{cases} \tag{2.32}$$

The formation and possible shedding of the vortex rings appears to be a major energy dissipation mechanism, and it is the one responsible for the observed increase in resonator losses. The frictional wall losses are constant while the jet losses are amplitude dependent and they dominate the constant resistance term during high-amplitude oscillations.

2.2.4 Power reflection and power transmission coefficients

In this section the influence of the implementation of a Helmholtz resonator in a duct is studied. Considering a duct with traveling incident and reflected sound waves given by [5]:

$$p_i = P_i e^{i(\omega t - k_w x)} \tag{2.33}$$

$$p_r = P_r e^{i(\omega t + k_w x)} \tag{2.34}$$

then from one-dimensional acoustic theory [5]:

$$R_\Pi = \left|\frac{P_r}{P_i}\right|^2 = \frac{(\rho_0 c/2S)^2}{(\rho_0 c/2S + R)^2 + X^2} \tag{2.35}$$

$$T_\Pi = 1 - R_\Pi = \frac{R^2 + X^2}{(\rho_0 c/2S + R)^2 + X^2} \tag{2.36}$$

where R_Π and T_Π are the power reflection and power transmission coefficients, respectively, and R and X are the resistive and reactant part of the resonator acoustic impedance $Z = R + iX$.

The power transmission coefficient represents quantitatively the energy of the incident wave that got past the resonator, meaning that for $T_\Pi = 0$ all energy is redirected back to the source (the resonator is in resonance) and for $T_\Pi = 1$ means the impedance is infinite (being the same as a wall) and so all energy moves downstream past the resonator.

2.3 Influence of cavity geometry

2.3.1 Cavity shape

The lumped method for the estimation of the resonant frequencies of Helmholtz resonators is obtained assuming that the only oscillating mass responsible for the vibration response of an acoustic perturbation is concentrated on the neck, and that the mechanical analog of the spring is constant and directly proportional to the volume of the cavity of the resonator. In practice such assumptions are not accurate since many secondary phenomena can occur. The theory of Helmholtz resonators was generalized by Alster [3] to include the effects of motion of particles and pressure fluctuations inside the cavity, as well as the effect on its geometry. Since some applications require different configurations for the volume, several fundamental geometries were studied. The theory is valid - not only for Helmholtz resonators - but also for several different shapes, such as the closed branched tube (the so-called λ/4 resonator). After several tests with Helmholtz resonators performed by Alster significant discrepancies as high as 30% between measured and calculated resonant frequencies using the classical theory were observed. Searching for the cause of the error led to a conjecture that the theory was much too simplified and consequently not reliable enough for more precise calculations. Although lumped theory can give a good approximation of the characteristics of the resonator, it can only be seen as a starting point since the assumptions made don't take into account the cavity geometry. For example, a one liter of volume (typical empty bottle) filled one-quarter with water can show different resonant frequencies depending on being in the horizontal or vertical position, therefore proving that the shape of the resonator is a key factor.

The theory proposed by Alster [3] assumes that the gas is moving not only in the neck but through the whole volume of the resonator, as stated before. As a starting point, it is assumed that the resonator is symmetrical around the axis of the neck. The streamlines inside the volume follow an almost potential-like flow having the following representation [3]:

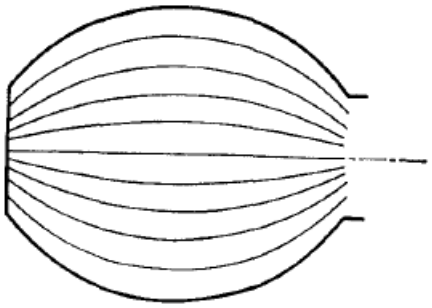

Figure 2.13: Streamlines inside the cavity volume [3]

The improved formula for the resonant frequency of the resonator proposed by Alster is [3]:

$$f_0 = \frac{c}{2\pi}\sqrt{\frac{S}{1,21(V+V_n)\{\frac{V}{V+V_n+V_{01}}\frac{h}{h+l+l_{01}}[l_v+(l+l_{01})(1+\frac{1}{2}[\frac{V_n+V_{01}}{V}+\frac{l+l_{01}}{h}]+\frac{1}{3}\frac{V_n+V_{01}}{V}\frac{l+l_{01}}{h})]+l_{02}\}}} \tag{2.37}$$

where h is the height of the resonator from the bottom to the neck, V_n is the volume of the neck, l_{01}, l_{02} are two parts of the total end-correction length due to the motion of gas particles outside the resonator and V_{01} is the volume of the hypothetical elongation of the neck due to the motion of gas.

Equation (2.37) is to be compared with the classical formula given by equation (2.24):

$$f_0 = \frac{c}{2\pi}\sqrt{\frac{S}{Vl'}} \tag{2.38}$$

This theory suggests that the influence of cavity geometry effect is included on an end term correction for the inner side of the neck, given by [3]:

$$l_v = \frac{S}{Vh}\int_0^h \frac{xV(x)}{S(x)}dx \tag{2.39}$$

where $V(x)$ is the total volume of the resonator at x and $S(x)$ is the area variation of the resonator along x.

With this formula it is possible to determine the resonant frequencies of symmetric resonators with any varying shape, assuming that D $\leq \lambda$/4 (so that there is no multi-dimensional interaction) and $h \geq 2a$, where D is any dimension of the resonator. Several shapes and form factors of fundamental geometries are presented as an example in figure 2.14 [3].

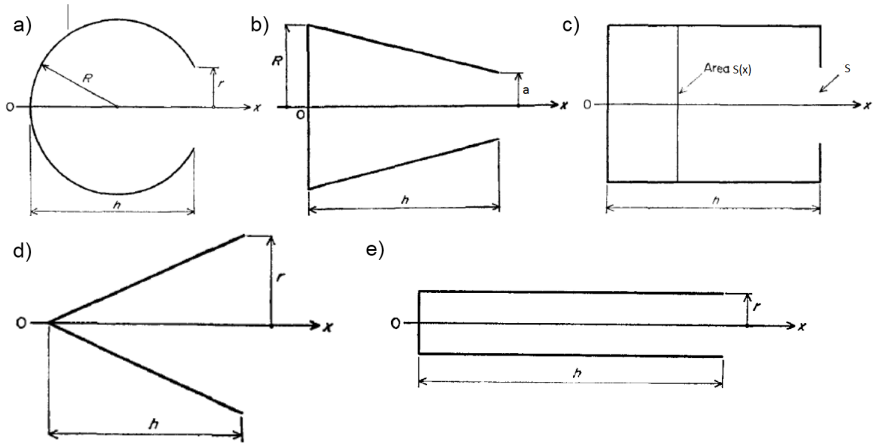

Figure 2.14: Fundamental geometries; (a) Sphere (b) Frustum of Cone (c) Prism (d) Cone (e) λ/4 resonator adapted from [3]

- Sphere: $l_v = \frac{r^2}{R}\frac{1}{2-A}\left[\frac{1}{3} - \frac{1}{2(A+1)} - \frac{2}{(A+1)^2} + \frac{4}{(A+1)^3} ln\frac{2}{1-A}\right]$, $A = \sqrt{1-(r/R)^2}$
- Frustum of Cone: $l_v = \frac{h}{(R/r)^2+(R/r)+1}[\frac{1}{3} - \frac{1}{2}\frac{R}{R-r} + (\frac{R}{R-r})^3(\frac{R}{r} - 1 - ln\frac{R}{r})]$
- Prism: $l_v = \frac{S}{S(x)}\frac{h}{3}$
- Cone: $l_v = h/3$
- λ/4 resonator: $l_v = h/3$

In order to compare this formula to the classical approach, some values of resonant frequencies for different geometries and the corresponding error to the new formula are given below according to [3]:

Resonator	Resonant frequency (classical) [Hz]	Error [%]
Sphere	169	6,11
Frustum of cone	183	50
Cylinder with lateral hole	154	13,5
Cylindrical prism	163	9,95
Cylindrical prism (long neck 1)	148	11,9
Cylindrical prism (long neck 2)	257	14,6
$\lambda/4$ resonator: 50 cm	411	143,1

Table 2.1: Comparison of measured resonant frequencies with classical formula predictions [3]

2.3.2 Length-to-Width ratio

Since most applications require different geometries of the cavity to fit in an integrated product, the present section pursues one of the special cases of one-dimensional limit for small cavity length-to-diameter ratio, as the volume approaches a ”pancake” configuration. For an inviscid one-dimensional radial propagation, the solution was studied by Dickey and Selamet [21].

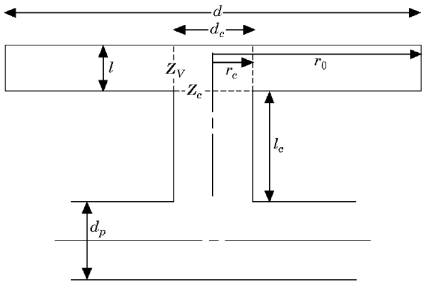

Figure 2.15: Geometry of the ”pancake” configuration [21]

As d approaches d_c a one-dimensional axial wave propagation in the cavity may be assumed. As l/d is reduced toward and below unity, the effects of the non-planar wave propagation are expected to increase, thereby requiring a multi-dimensional analysis that takes into account the radial and axial directions. However, as the *l/d* ratio is decreased further, such that the volume approaches a ”pancake” configuration, as shown in figure 2.15, axial gradients in the volume become negligible and a one dimensional solution may be obtained, in which purely radial propagation in the volume is considered.

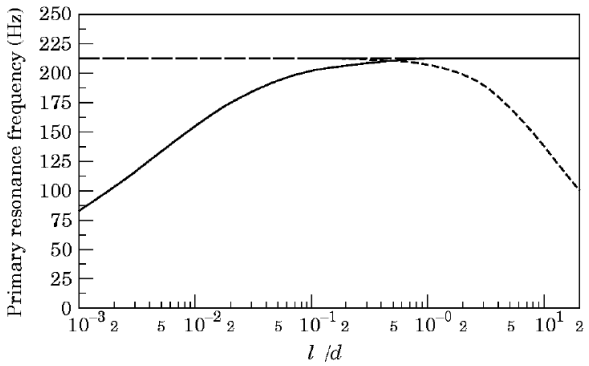

Figure 2.16: The primary resonance frequency of concentric Helmholtz resonator from 1-D radial (——), 1-D axial (- - -) and lumped volume (— —) analyses. $V = 1000\ cm^3$, $a = 2\ cm$, $l = 8\ cm$ [21]

A reduction in the primary resonance frequency for low values of *l/d* is clearly shown in figure 2.16, proving that if *l/d* is increased approaching the order of unity, all three methods tend to yield similar results. These results also corroborate with the research of Alster [3] presented before, proving that the same volume with a different configuration will produce a different resonant frequency. It should be also noted that with further increase in *l/d* axial propagation begins to dominate and, as the volume length l becomes very small, the effects of viscosity which are neglected in the present study are expected to become significant.

2.3.3 Variable volume in time

The most common decision to tune a Helmholtz resonator is to change the geometry of the resonator's orifice in order to change the effective mass and resistance present in the neck, however this approach is strongly dependent on the complex fluid dynamics of the flow entering the orifice. Another approach

suggested by Horowitz et al. [22] is to develop an electromechanical acoustic liner to tune the acoustic impedance. By adding this new degree of freedom to the system a flexible membrane instead of a rigid wall at the bottom of the cavity volume of the Helmholtz resonator can be tuned to react to a resonant frequency of choice. Since the impedance of the backplate can be adjusted electromechanically, the input impedance and natural frequencies of the resonator can be tuned to a desired value. In the study performed by Horowitz et al. [22] two backplates thicknesses were considered: 0.025 mm and 0.127 mm.

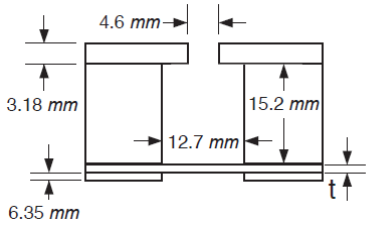

Figure 2.17: Cross-section of prototype compliant-backplate Helmholtz resonator, where the backplate thickness, t, is 0.127 mm and 0.025 mm for the two backplates, respectively [22]

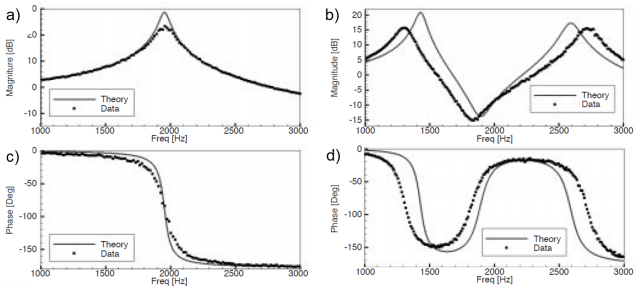

Figure 2.18: a) Magnitude of the pressure amplification obtained for the Helmholtz resonator with the 0.127 mm backplate; b) Magnitude of the pressure amplification obtained for the Helmholtz resonator with the 0,025 mm backplate; c) Phase of the pressure amplification obtained for the Helmholtz resonator with the 0,127 mm backplate; d) Phase of the pressure amplification obtained for the Helmholtz resonator with the 0,025 mm backplate [22]

In the 0.127 mm backplate the results show a behavior similar to a conventional rigid walled resonator, with a single peak occurring in the frequency range tested (resonance frequency), meaning that in this situation the system doesn't have two degrees of freedom. In the other case, the 0.025 mm backplate is sufficiently thin and flexible to generate two amplification peaks at the two resonant frequencies. The first resonance peak occurs around 1325 Hz and the second at 2730 Hz. Therefore, by adding a thin layer in the resonator cavity along with a controller of the resistance capacity of this membrane, it is possible to obtain an active control of the resonator's behavior.

Note that the current study was limited to incident SPL of less than 80 dB to assess the accuracy of the lumped element model in the absence of nonlinear effects, however in engineering applications the SPL in engine ducts can reach 160 dB which implies that in this model a non-linear resistance should be added to the neck resistance. There is also the possibility that the membrane may not be able to withstand such large values of pressure fluctuations in the cavity and it may burst for very high SPL.

Finally the values of resistance and reactance for each case are presented in the following figure 2.19:

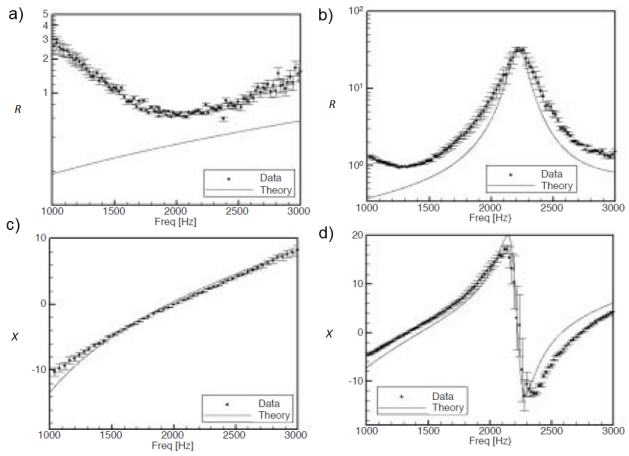

Figure 2.19: a) Normalized specific acoustic resistance obtained for the Helmholtz resonator with the 0.127 mm backplate; b) Normalized specific acoustic resistance obtained for the Helmholtz resonator with the 0.025 mm backplate; c) Normalized specific acoustic reactance obtained for the Helmholtz resonator with the 0.127 mm backplate; d) Normalized specific acoustic reactance obtained for the Helmholtz resonator with the 0.025 mm backplate [22]

It can be seen that the measured values of resistance were higher than predicted, especially in the low frequency range for the 0.127 mm backplate. This suggests the possible existence of measurement issues with the experimental setup or perhaps unmodeled dynamics, but the reactance part seems to be in good agreement with predictions.

2.4 Influence of neck geometry

2.4.1 Extended neck

This section outlines the main conclusions of the work of Selamet and Lee [12], regarding the influence of the length, shape and the perforation porosity of the neck extension on the resonance frequency and transmission loss. It is shown that the Helmholtz resonator may be controlled by these geometrical parameters of the neck without changing the cavity volume.

Due to volume constraints in most engineering applications (aerospace, automobile, etc) the application of low-frequency resonators is often impossible. Therefore, the resonance frequency must be lowered without increasing the cavity volume.

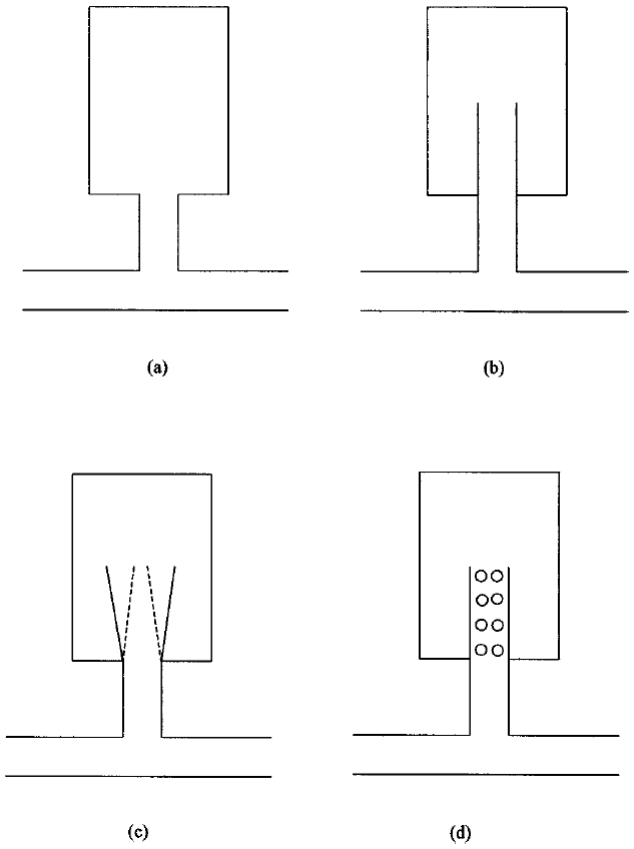

Figure 2.20: (a) represents the typical Helmholtz resonator with no neck extension, (b) represents an extension into the volume cavity, (c) represents a conical extension into the volume cavity, (d) represents a perforated neck extension into the volume cavity [12]

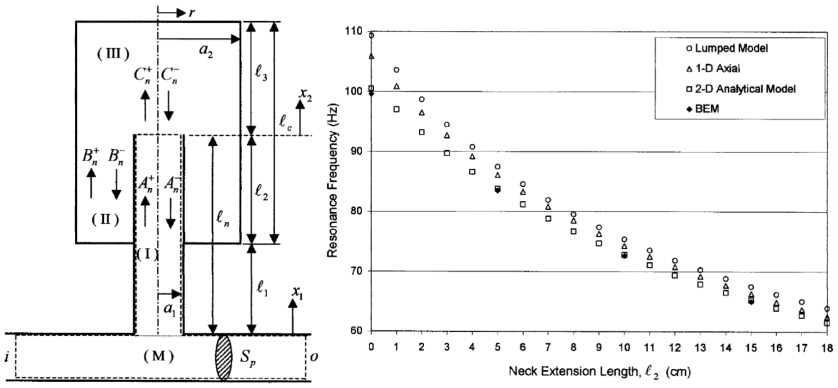

Figure 2.21: Resonator nomenclature (left), Resonance frequency predictions with various neck extension lengths $l_1 = 8.5\ cm$ (right) [12]

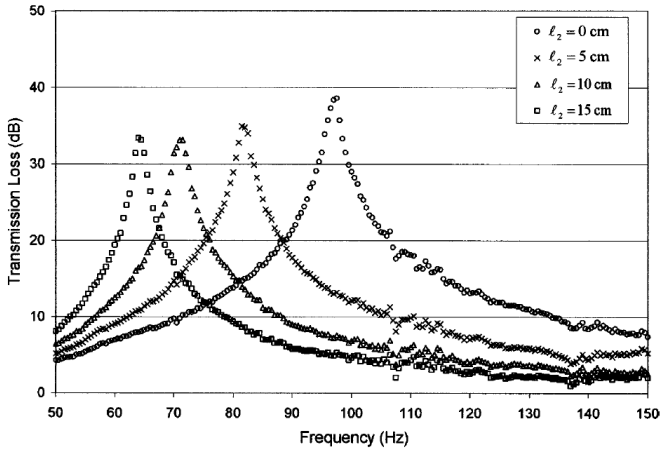

Figure 2.22: Measured Transmission loss for $l_1 = 8.5\ cm$ and several neck extension [12]

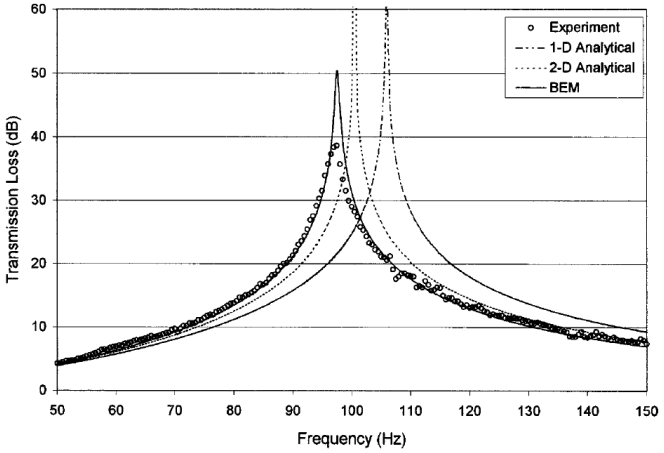

Figure 2.23: Measured vs. Calculated Transmission loss for $l_1 = 8.5\ cm$ and $l_2 = 0\ cm$ [12]

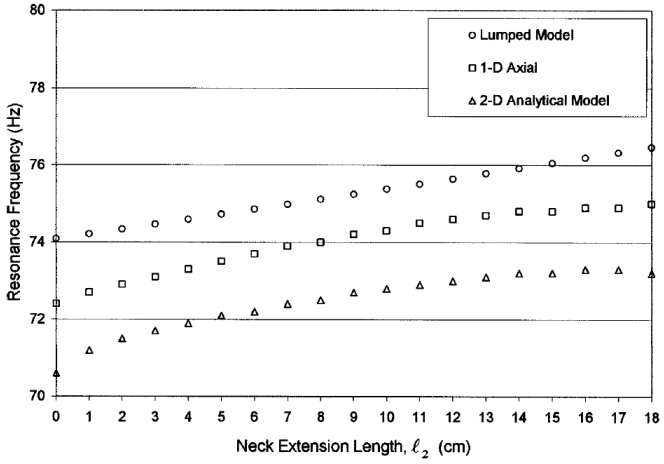

Figure 2.24: Predicted resonance frequencies for fixed length $l_1 + l_2 = 18.5\ cm$ [12]

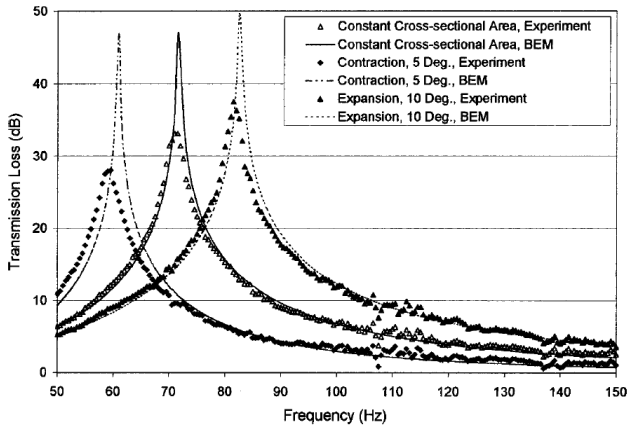

Figure 2.25: Measured vs. Calculated Transmission loss for $l_1 = 8.5\ cm$ and $l_2 = 10\ cm$ with conical neck extension [12]

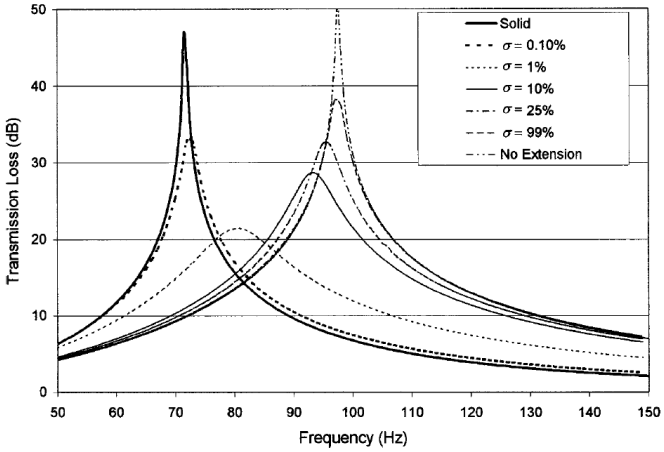

Figure 2.26: Measured vs. Calculated Transmission loss for $l_1 = 8.5\ cm$ and $l_2 = 10\ cm$ with perforated neck extensions [12]

Selamet and Lee [12] concluded in case (b) applying a neck extension into the volume lowers the resonance frequency and the attenuation band becomes narrower while keeping the transmission loss moderately unchanged (see figure 2.22). It was also observed that both the analytic and numerical models overestimate the transmission loss and that the analytical models overestimate the resonant frequency, due to the presence of higher frequency modes in the vicinity of neck. It is shown the influence on the side of the increase in neck length, meaning that the increase in the neck length to the outside or to the inner side (volume cavity) only deviates the resonant frequency in about 10%.

Regarding the conical extension and taking the constant cross section as a reference, figure 2.25 shows that in a five degree contraction the resonance frequency decreases about $\approxeq 20\%$ and the transmission loss $\approxeq 18\%$. On the contrary, in a ten degree expansion, the resonant frequency increases about $\approxeq 15\%$ and the transmission loss $\approxeq 12\%$. Finally for case (d) figure 2.26 shows that without extension, the resonant frequency matches with case (a), while applying a solid neck extension gives the case (b) as expected. The same figure shows that with perforated neck extension, as the porosity increases, the

resonance frequency increases and the magnitude of the transmission first decreases followed by an increase. The increase in transmission loss is related to a decrease in the resistance or damping of the perforation impedance.

2.4.2 Tapered neck

In this section, the work of Tang [14] regarding a Helmholtz resonator having an increasing neck area into the cavities, will be presented. Results show that significant improvement of the sound absorption capacity of the resonators can be obtained having a smooth increasing transition of the neck, also known as tapering. Such improvement is enhanced when the tapered length is increased.

The acoustic impedance at the outlet of the Helmholtz resonator affects significantly the achievable sound absorption coefficient if it is used as wall lining and sound transmission loss if it is applied to a duct. The highest absorption takes place near the resonance frequency and the extent of the effect therefore depends on the resistance part of the acoustic impedance. Since a smoother area change from the neck towards the cavity will reduce the flow resistance, tapering the neck suggests to be a way to enhance the performance of a Helmholtz resonator without significant alteration of geometry. However, the resonant frequency may be affected by the tapering and a new equation for the resonant frequency of the resonator is given by [14]:

$$f_0 = \frac{c}{2\pi}\sqrt{\frac{\pi r_i^2}{L_n V}\left[\frac{r_i L}{r_o L_n}\left(1+\frac{\pi r_0^2 L_p}{V}\right)+\frac{L_p}{L_n}\right]^{-1}} \tag{2.40}$$

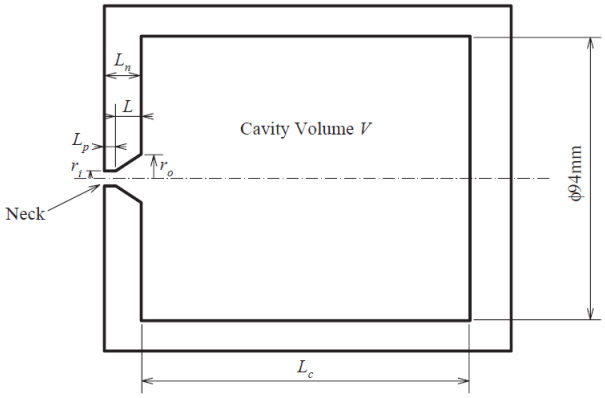

Figure 2.27: Schematics of the Helmholtz resonator with tapered neck [14]

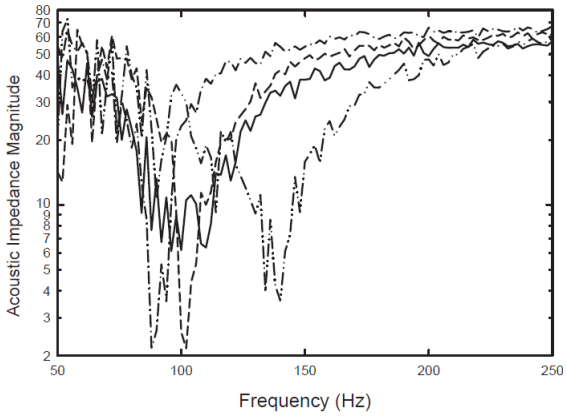

Figure 2.28: Acoustic impedance magnitudes; — ·· — : L_c = 100 mm, 85% tapered; – – – : L_c = 160 mm, 85% tapered; — · — : L_c = 220 mm, 85% tapered; —— : L_c = 100 mm, 0% tapered (reference). L_n = 5,3 mm, r_i = 2,5 mm [14]

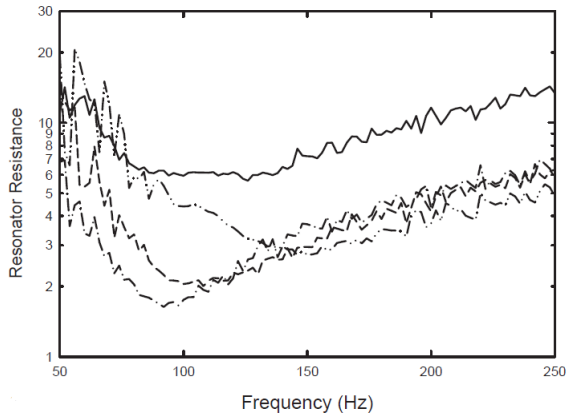

Figure 2.29: Resistance magnitudes; — ·· — : L_c = 100 mm, 85% tapered; – – – : L_c = 160 mm, 85% tapered; — · — : L_c = 220 mm, 85% tapered; —— : L_c = 100 mm, 0% tapered (reference). L_n = 5,3 mm, r_i = 2,5 mm [14]

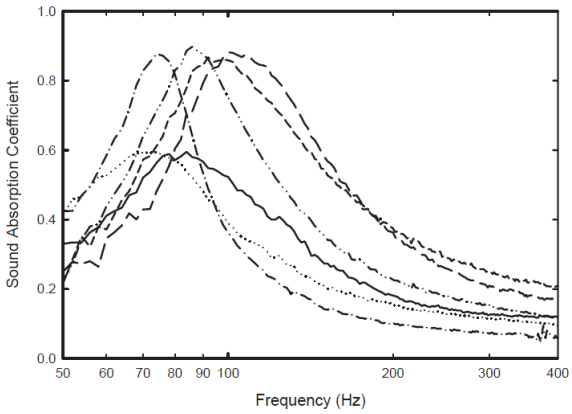

Figure 2.30: Sound absorption coefficient magnitude; — ·· — : L_c = 100 mm, 85% tapered; – – – : L_c = 160 mm, 85% tapered; — · — : L_c = 220 mm, 85% tapered; —— : L_c = 100 mm, 0% tapered (reference). L_n = 5,3 mm, r_i = 2,5 mm [14]

Figure 2.30 shows the comparing of the sound absorption of the Helmholtz resonator with and without the neck tapering. It can clearly be seen that tapering the neck causes a large increase in the sound absorption, as high as 40%.

The above conclusions and results may not apply to the case where the neck inlet is larger than its outlet, that is $r_i > r_0$. The resonance frequency will still be increased if one uses the frequency corresponding to the cavity inlet area of πr_0^2 as the reference, which is a trivial choice due to the manufacturing process. Tapering in this case increases the viscous resistance but the radiation resistance at the neck inlet is reduced. The condition $r_i > r_0$ is not recommended as it tends to introduce additional flow separation at the neck inlet.

As shown in the previous figures the experimental data reveal a large decrease in the resistive part of the impedance, leading to an increase of the absorption coefficient of about 20%. The tapering has reduced more than 60% of the impedance in the untapered condition. The deeper the tapering, the higher the sound absorption.

2.4.3 Spiral neck

In this section the study of Shi and Mak [23] for the Helmholtz resonator with a spiral neck is presented. Since in most applications there are space constraints a spiral neck is tested to understand the new design. The curvature effect of the spiral neck is transformed to an equivalent straight tube and the overall attenuation performance of the Helmholtz resonator is then derived. The theoretical results agree well with the simulation predictions of a Finite Element Element method (FEM), showing that a Helmholtz resonator with a spiral neck can achieve high sound reduction within a small space at low frequencies.

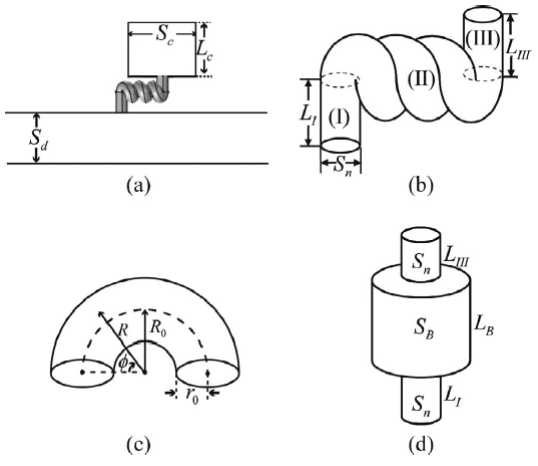

Figure 2.31: (a) A HR with a spiral neck; (b) The spiral neck with three turns; (c) A section of the curved duct; (d) The equivalent of the spiral neck [23]

Results also show that the resonance frequency of the Helmholtz resonator can be reduced, which has potential applications in tonal noise control in a limited space.

The geometries of the duct system are as follows; Sc = 36π cm^2, Lc = 10 cm, Sd = 144 cm^2, Lb =

100 cm, Sn = $\pi\ cm^2$, L_I = 3 cm, L_{III} = 3 cm, R_0 = 1.2 cm, and r_0 = 1 cm.

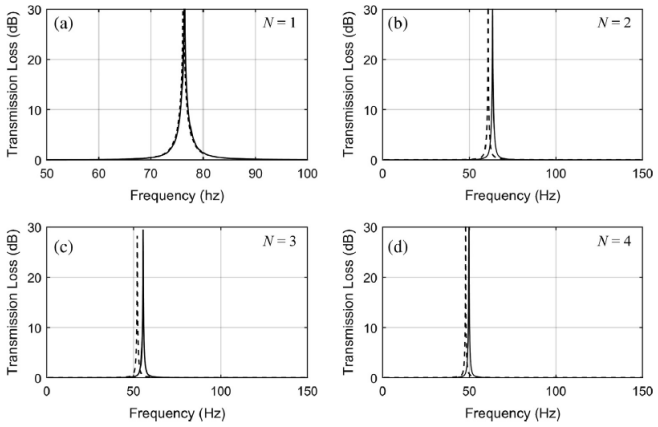

Figure 2.32: Transmission loss of the HR with a spiral neck (solid lines represent the results of theoretical prediction and dashed lines those of the FEM simulation) for a number of N turns [23]

Including more turns for the spiral neck can shift the resonance frequency much lower. Apart from its low-frequency performance, the proposed resonator also has several resonance frequencies at higher frequencies because of the long neck that can reach a dimension comparable with the sound wavelength being considered. It is therefore very useful when the noise source contains more than one frequency to be controlled, which is the case of fan noise where the frequency is determined by the speed of the fan rotation [23].

2.5 Influence of arrangement

2.5.1 Series arrangement

With the aim of having a Helmholtz resonator with two degree of freedom, Xu et al. [24] studied the acoustic characteristics of a dual Helmholtz resonator which consists of a pair of cylindrical neck and cavity connected in series (neck–cavity–neck–cavity). The theoretical resonance frequencies and transmission loss from the lumped model agree well with the analytical results of a two-dimensional model, while showing a reasonable comparison with both the numerical predictions of a Boundary Element Method (BEM) and the measurements [24].

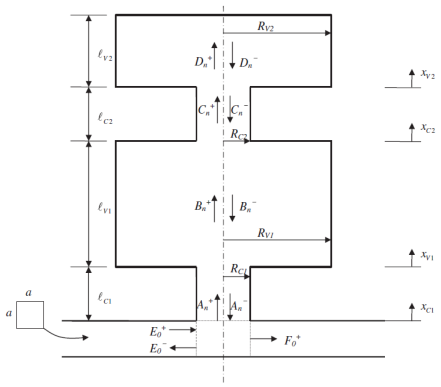

Figure 2.33: Schematics of the Dual Helmholtz resonator [24]

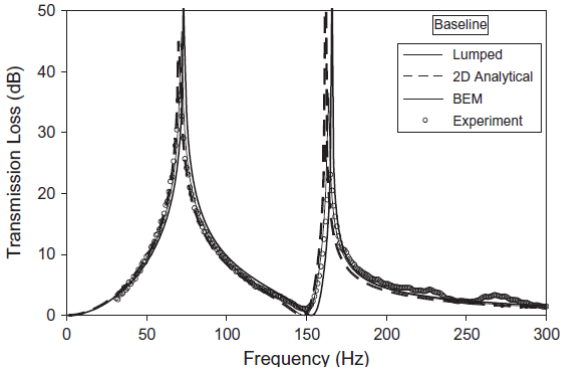

Figure 2.34: Transmission loss of the "baseline" dual Helmholtz resonator from lumped parameter theory, 2D analytical predictions, BEM, and measurements (C1 = 2 cm, V1 = 7.62 cm, C2 = 1.75 cm, V2 = 7.62 cm, l_{C1} = 8.5 cm, l_{V1} = 20.32 cm, l_{C2} = 7.62 cm, and l_{V2} = 10.16 cm) [24]

This system behaves as two combined mass-spring systems in series arrangement. Figure 2.34 shows that both transmission loss peaks are observed at the resonance frequencies (73 and 166 Hz). There is also a frequency in between where the transmission loss is nearly zero, suggesting an anti-resonance behavior. Deviations in the magnitude of the transmission loss between the lumped approach and experiments may be observed in the immediate vicinity of resonance frequencies. Such deviations may be attributed to the neglect of viscous damping in the Helmholtz resonator as well as the finite input power available to acoustic drivers in the experimental setup.

The resonance frequencies decrease with the increasing length of the 2nd neck, decreasing radius of the 2nd neck, and increasing volume of the 2nd cavity; while the influence of the shape of the 2nd cavity (diameter to length ratio) remains small.

The first resonance frequency may also be lowered with decreasing the ratio of both volumes (V1/V2) while retaining the total volume of the two cavities. The variation in the first resonance frequency is observed to be smaller than the second one and, through variation of neck lengths, the width of the transmission loss can be adjusted, while keeping the peak frequencies the same. Such flexibility could prove to be helpful particularly when dealing with space constraints in a variety of engineering applications.

2.5.2 Parallel arrangement

In this section a parallel arrangement of necks connected to a cavity is studied. Using the assumptions of lumped theory this system can be seen as an Helmholtz resonator with multiple necks. The aim of this study is simulate the response of the system, namely to find its natural frequency and absorption coefficient.

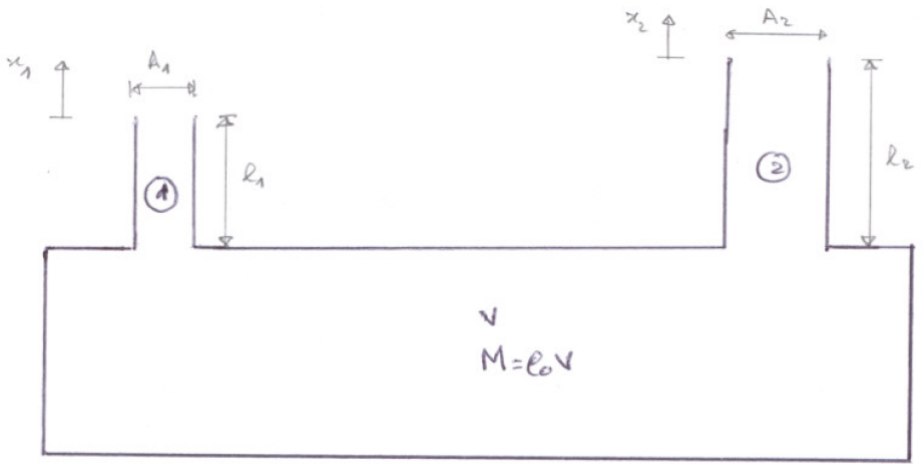

Figure 2.35: Schematics of the Parallel Helmholtz resonator

Using Newton's second law of motion yields:

$$\begin{cases} m_1 \frac{d^2x}{dt^2} = A_1 \Delta p = A_1 \int \frac{dp}{d\rho} d\rho = A_1 \int c_0^2 d\rho = A_1 c_0^2 \Delta\rho \\ v = \frac{1}{\rho} \Rightarrow dv = -\frac{d\rho}{\rho_0^2} \Leftrightarrow d\rho = -\rho_0^2 dv \Rightarrow \Delta\rho = -\rho_0^2 \Delta v \\ \Delta v = \frac{\Delta V}{M} = \frac{A_1 x_1 + A_2 x_2}{M} = \frac{A_1 x_1 + A_2 x_2}{\rho_0 V} \end{cases} \tag{2.41}$$

Knowing that $m_1 = \rho_0 A_1 l_1$ gives:

$$\frac{d^2x_1}{dt^2} = -\frac{c_0^2 l_0^2 A_1}{\rho_0 A_1 l_1} \frac{A_1 x_1 + A_2 x_2}{\rho_0 V} \Leftrightarrow \frac{d^2x_1}{dt^2} = -\frac{c_0^2}{l_1 V}(A_1 x_1 + A_2 x_2) \Leftrightarrow \frac{d^2x_1}{dt^2} + \frac{c_0^2 A_1}{l_1 V} x_1 + \frac{c_0^2 A_2}{l_1 V} x_2 = 0 \tag{2.42}$$

For the second tube a similar equation is obtained:

$$\frac{d^2x_2}{dt^2} + \frac{c_0^2 A_1}{l_2 V} x_1 + \frac{c_0^2 A_2}{l_2 V} x_2 = 0 \tag{2.43}$$

Considering that $x_1 = X_1 e^{i\omega t}$, $x_2 = X_2 e^{i\omega t}$ and after some mathematical manipulation gives:

$$\omega_0 = \frac{c_0}{\sqrt{V}} \sqrt{\frac{A_2}{l_2} + \frac{A_1}{l_1}} \tag{2.44}$$

Taking into account the motion of fluid outside the neck that moves in unison with the fluid in the neck, length l_i should be replaced by l_i' given by equations (2.6) and (2.6). For n necks the resonance frequency is:

$$\omega_0 = \frac{c_0}{\sqrt{V}} \sqrt{\sum_{n=1}^{n} \frac{A_n}{l_n'}} \tag{2.45}$$

2.6 Applications

2.6.1 Micro Helmholtz Resonator for Ultrasonic Distance Sensor

The Helmholtz resonator is mostly seen as device to absorb sound in most applications, however it can also be used to amplify it. Implementation of a Helmholtz resonator in a micro sensor in order to increase it's sensitivity seems to be a tempting research. More specifically, this study from Suzuki et al. [25] shows the influence of a Helmholtz resonator in the sensitivity of an ultrasonic distance sensor, which basically consists of a piezoresistive cantilever microphone that transforms an acoustic wave into a resistance change. A Helmholtz resonator of 600 μm height achieve to make the maximum amplitude of the cantilever vibration 17.5 times larger. Suzuki et al. [25] also evaluated the dependence of the resistive sensitivity on frequency and acoustic pressure. The micro sensor attached to a Helmholtz resonator was able to detect the distance of 0.5-6.0 m with the maximum error of 2.0%. In this particular study the cantilever has a thickness of 0,3 μm and a resonance frequency of 23,6 kHz while the Helmholtz resonator was designed with a resonant frequency of 22,6 kHz using lumped theory.

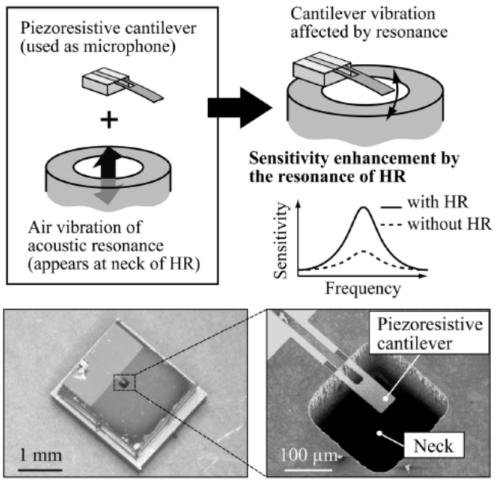

Figure 2.36: Schematic view of the sensitivity-enhancement principle with photographs of the fabricated sensor [25]

The main principle behind the insertion of the Helmholtz resonator in the sensor is that the air fluctuations caused by the Helmholtz resonator, close to the neck and near resonance, cause a larger displacement on the cantilever, which becomes more sensible to feeble sounds and vibrations. Figure

(2.36) shows the schematics of the enhancement. The center of mass of the cantilever is placed at the geometric center of the neck. The resonant frequency of the cantilever is close to the resonant frequency of the resonator.

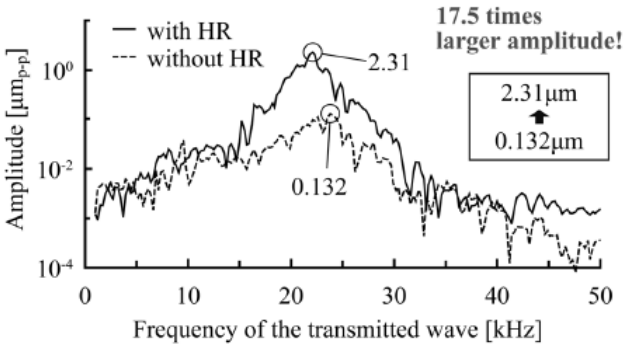

Figure 2.37: Vibration amplitude at the tip of cantilever against single frequency wave [25]

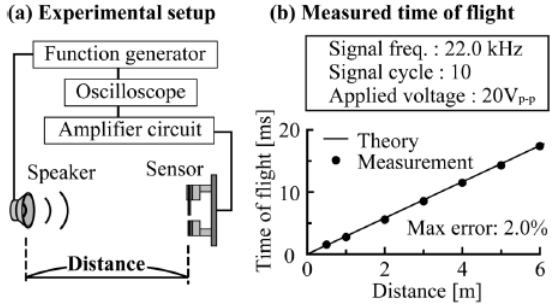

Figure 2.38: (a) Experimental setup for basic distance measurement. (b) Time of flight measured by the sensor with Helmholtz resonator [25]

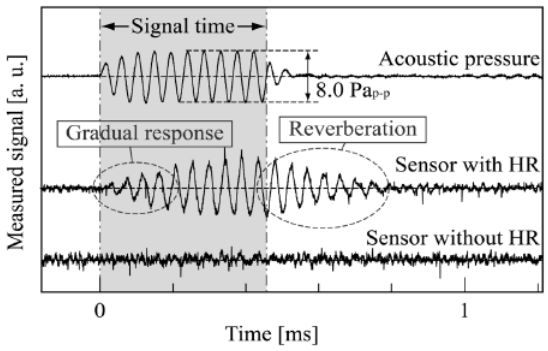

Figure 2.39: Signal forms of the sensor with/without Helmholtz resonator measured by detecting the same ultrasonic waves. The acoustic pressure at the sensor position is added. The grey area shows the signal time [25]

Figure 2.37 shows the vibration amplitude at the tip of cantilever with and without the influence of the Helmholtz resonator. The acoustic pressure at the sensor position was 1.9 Pa_{p-p}. The largest amplitude of the cantilever with Helmholtz resonator was 2.31 μm_{p-p}, and without Helmholtz resonator was 0.132 μm_{p-p} meaning that attaching an Helmholtz resonator achieved to make the maximum amplitude of the

cantilever vibration 17.5 times larger than the previous case.

Figure 2.39 shows the influence of the Helmholtz resonator in the measured signal. It can clearly be seen that the signal of the sensor without Helmholtz resonator was buried in the background noise whereas, with the Helmholtz resonator, the sensor detects the sound wave more easily. It can also be seen some reverberation in the response with Helmholtz resonator, but this is caused by the resonance of the sensor. The effect of the signal form, however, caused no serious error for the detecting distance at our measurement condition.

2.6.2 Tunable Acoustic Absorber Using A Micro Acoustic Hole Array

In this last part the work of Konishi et al. [26] regarding a MPP (multi-perforated plate) consisting of an array of microholes with a variable cavity volume is presented.

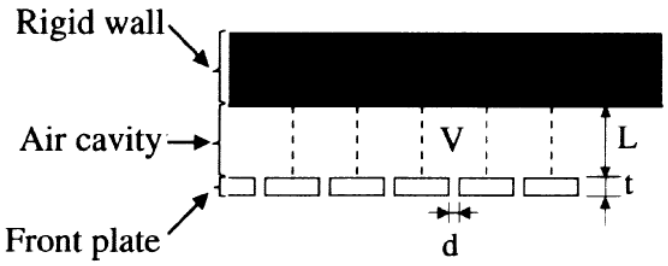

Figure 2.40: Equivalent structure of Helmholtz resonator [26]

The Rigid wall in this case can be moved forwards or backwards, varying the volume V of the air cavity, and so adjusting the resonant frequency of the system to a desirable value. Increasing the volume the resonant frequency lowers as expected and it is shown that the absorption coefficient also increases. In this particular as depicted in figure 2.41 case the diameter of the holes is 100 μm.

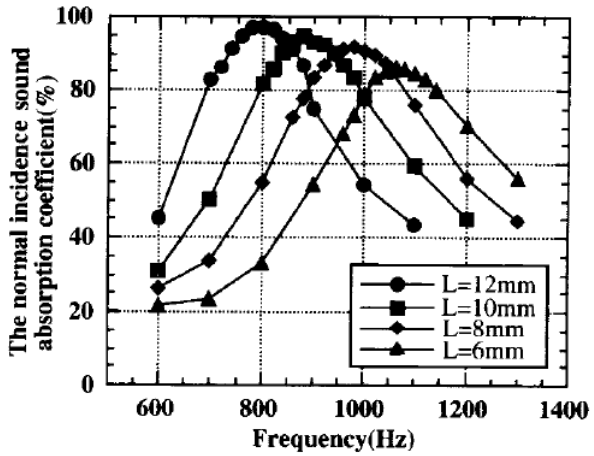

Figure 2.41: Frequency response of the normal-incidence sound absorption coefficient α_0 at various distances of air cavity [26]

Chapter 3

Mathematical model

In the following sections a discussion about the changes to the model with the presence of the metal plate is presented. The metal plate is a thin metal sheet ($\approx$ 0,5mm) made of stainless steel with holes created from a laser.

This new theory involves around the concept of impedance - the introduction of the metal plate can be modeled as a new impedance on the system of the Helmholtz resonator. This approach brings theoretical results which corroborates with experimental data under certain conditions.

3.1 Helmholtz model with MPP

After the literature review and research about the current technology of Helmholtz resonators has been conducted, the introduction of the metal plate is studied. The mathematical model is presented along with the transfer functions and assumptions/approximations utilized in the study. Figure 3.1 shows a schematic example of the resonators with MPP:

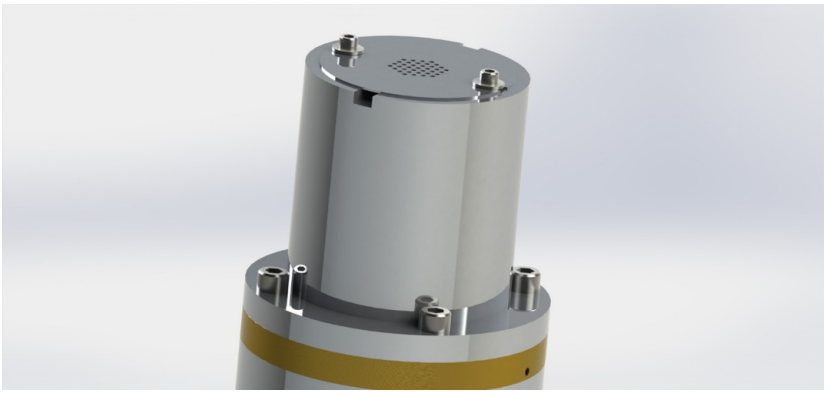

Figure 3.1: Helmholtz resonator with multi-perforated plate

3.1.1 Impedance model

The introduction of the metal plate near the resonator neck acts as an additional impedance added to the impedance of the resonator. The impedance of the metal plate can be taken from micro-perforated panel theory initially proposed by Maa [27]:

$$Z_{MPP} = Z_0(R_{MPP} + iX_{MPP}) \tag{3.1}$$

where $Z_0 = c/S$ is the specific acoustic impedance.

In equation (3.1) the real part is the normalized specific acoustic resistance given by

$$R_{MPP} = \frac{32 t_p \mu}{\sigma \rho_0 c d_p^2} \left(\sqrt{1 + \frac{k_p^2}{32}} + \frac{\sqrt{2}}{32} k_p \frac{d_p}{t_p} \right) \tag{3.2}$$

and the imaginary part is the normalized specific acoustic reactance given by

$$X_{MPP} = \frac{\omega}{c} \frac{t_p}{\sigma} \left(1 + \frac{1}{\sqrt{9 + \frac{k_p^2}{2}}} + 0,85 \frac{d_p}{t_p} \right) \tag{3.3}$$

where $k_p = (d_p/2)\sqrt{\rho_0 \omega / \mu}$ (which is essentially the Shear number described by Muttalip [19]) is proportional to the ratio of the radius to the viscous boundary layer thickness inside the orifice, μ is the absolute viscosity coefficient, ω is the angular radian frequency, t_p is the thickness of the MPP, d_p is the hole diameter and σ is the porosity, which is defined as the area of all holes divided by the area of the neck. However, since the current application of this theory demands different units for the impedance, Z_0 will be modified in order to obtain the dimensions of kg/s, and it becomes $Z_0 = \rho_0 c S$.

The impedance described by Maa [27] has two contributions. By looking at the term in parenthesis in the previous equations, the first term corresponds to the oscillating mass of air within the neck (with the influence of the boundary layer) and the second term represents the end correction terms due to the oscillating mass of air around the neck. This characteristic is also found on the impedance of the Helmholtz resonator, where the oscillating air on the neck influences the air around. Adding this impedance Z_{MPP} to the impedance of the Helmholtz resonator Z_{HR} given by equation (2.23) gives:

$$Z_{Total} = Z_{HR} + Z_{MPP} \tag{3.4}$$

Starting with the original formula for the Helmholtz resonator given by equation (2.17) and adding the impedance of the MPP the response of the system becomes:

$$\xi_0 = \frac{1}{i\omega} \frac{SP}{b + i(\omega m - \frac{k}{\omega}) + Z_{MPP}} \tag{3.5}$$

The metal plate sheets are defined by the porosity σ and the perforation ratio ϕ. Porosity is defined as the total area of the perforated holes divided by the area of the neck. Since the resonators have different necks the same plate will have different values for each case. Perforation ratio is the area of a single hole divided by the polygon area where it is inserted, which gives the influence between hole interaction.

$$\sigma = \frac{nS_f}{S} \tag{3.6}$$

$$\phi = \frac{S_f}{S_a} \tag{3.7}$$

where n is the numbers of holes of the plate, S_f is the area of a single hole, S_a is the area of the polygon where it is inserted in and S is the neck area of the resonator, as shown in figure 3.2:

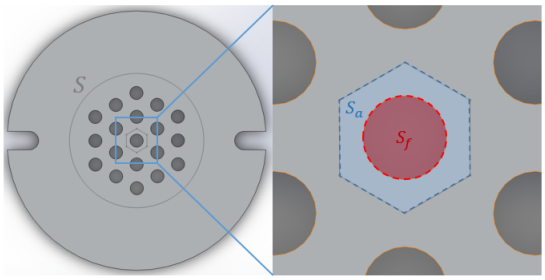

Figure 3.2: Metal plate schematics

The transfer function is useful to obtain the system's response to any given harmonic perturbation. The transfer function for the system with the metal plate impedance can be obtained from equation (3.5) which gives:

$$\frac{P_c}{P} = \left(\frac{\rho_0 c^2 S^2}{i\omega V}\right)\left(\frac{\rho_0 c k_n^2 S^2}{(2\ or\ 4)\pi} + \frac{2m}{a}\left(\frac{\mu\omega}{2\rho_0}\right)^{1/2}\left(1+\frac{\gamma-1}{\sqrt{Pr}}\right) + \frac{32 t_p \mu S}{\sigma d_p^2}\left(\sqrt{1+\frac{k_p^2}{32}} + \frac{\sqrt{2}}{32}k_p\frac{d_p}{t_p}\right) + i\left(\omega\rho_0 S l' - \frac{\rho_0 S^2 c^2}{V\omega} + \frac{\omega t_p \rho_0 S}{\sigma}\left(1+\frac{1}{\sqrt{9+\frac{k_p^2}{2}}} + 0,85\frac{d_p}{t_p}\right)\right)\right)^{-1} \tag{3.8}$$

3.1.2 Theory Validity Regime

The theory presented about MPP in this article can only be applied to metal plates which follow certain conditions. The conditions are the following:

1. Hole distribution on the plate should be uniform
2. No interaction between holes ($\phi < 50\%$)
3. Holes of sub-milimiter size
4. Low porosity ($\sigma < 15\%$)

5. Linear regime (i.e. low amplitudes)

Chapter 4

Experiments

4.1 Setup

The installation is composed of mainly two parts: computing interface, and structural apparatus. The computing interface part consists of all computing hardware and software used in these experiments to obtain and process the signals from the microphone, while the structural apparatus consists of the physical structure where the microphone, speaker and resonators are mounted. The description of each part is present in the next following sections.

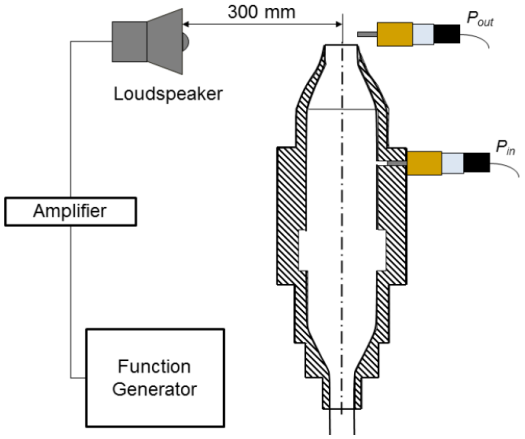

Figure 4.1: Resonator testing diagram. Adapted from [2]

4.1.1 Computing Interface

The computer was used for handling the programs of electronic instruments and for processing all the data obtained from experiments. The oscilloscope is a model '*Tektronix TDS 1001C-EDU*'. The signal generator is a model '*Tektronix AFG 3021b*'. The amplifier is a model '*ROTEL R8-890*' with a power of 150 W which amplifies the electric signal before entering the speaker. The Microphone device is a model '*Bruel and Kjaer type 2250*'. It is connected to the microphone and converts the pressure fluctuations into electric signals with a default gain. The default gain on the device is 10 dB but it can be adjusted.

The data acquisition board is a model '*Data Translation DT9841-VIB-SB*' and it receives, processes and sends signals obtained from experiments between the different instruments and has an acquisition frequency of 10000 Hz.

Turning now to the software side, two MATLAB programs were used in experiments: $main\_acq.m$ and $main\_proc.m$.

$Main\_acq.m$ is a program that controls the signals generated by the signal generator from the computer and produces a file with the signals acquired from the acquisition board. It was also designed to evaluate not only one frequency but an array of frequencies, so it was possible to obtain the frequency curves of the resonators. Frequencies and amplitudes are specified by the user, and each 15 seconds the program instructs the signal generator to run the next frequency step requested and records the signal received from the data board. It is essentially an acquisition data program.

$Main\_proc.m$ uses the data from $main\_acq.m$ and produces a transfer-function file by using FFT method which gives the amplitude and phase. However this program requires two files from $main\_acq.m$, because the result is non-dimensional, meaning the results obtained are relative between two given data points (remember the two-microphone method). Essentially, after generating the FFT files from the two files it uses a cross-correlation to obtain the amplitude and phase shifts between both signals, creating the desired frequency curves. It can be seen as a processing data program from $main\_acq.m$.

4.1.2 Structural Apparatus

The structural apparatus is presented in the following figure 4.2:

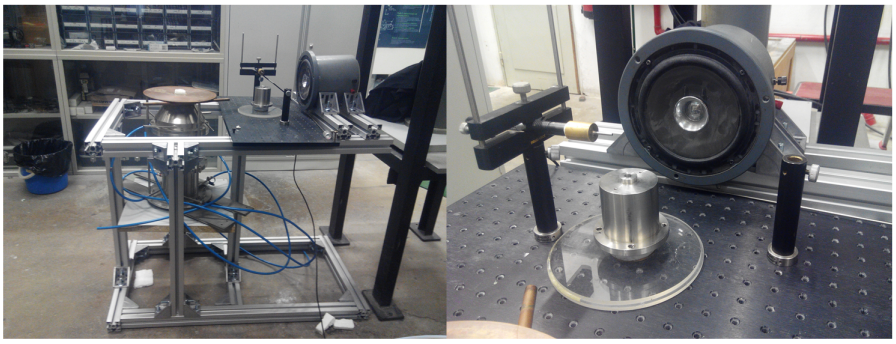

Figure 4.2: Structural Apparatus. Left - Full structure; Right - Testing area

The structure where the resonators, speaker and microphone are tested is built from aluminum bars, connected along bolted stainless steel joints. The installation was projected to withstand the 'big burner' presented in the picture and the other components. This installation was modeled in CAD using Solidworks and then built in the laboratory using an aluminum saw.

4.2 Signal Acquisition Process

In order to obtain experimental data, a microphone model '$B\&K\ Type\ 4189$' attached to a microphone amplifier model '$B\&K\ Type\ ZC0020$' was used to capture the acoustic perturbations by a speaker.

It is necessary to obtain two pressure data points from the resonator as shown in figure 4.1: one inside the cavity and one outside it. The inside data is obtained by coupling a pressure probe into the microphone tip in order to introduce the microphone into the cavity of the resonator. The probe is a small tube that measures pressure in the center. Several probes were available, and the longest ones - with around 10 cm - have shown larger dissipation and therefore more noise in the signal, which implies an increase in gain of the microphone for a better signal output. A 'good' signal obtained from the microphone is around 5-10 V_{p-p} (volts peak-to-peak), being 10 V_{p-p} the maximum the microphone can withstand. Due to this the shortest probe was used since it captures the least background noise using the default gain.

Initially the microphone with the probe is set inside the cavity and the signal generator is tuned using a rotating button to produce frequency that matches the resonant frequency of the resonator. The resonant frequency can be observed using the oscilloscope so that, in a matter of seconds when a peak in the voltage of the microphone is found, the resonance frequency is also found. Then a .xlsx (excel file) is used - which was previously created by the user - where it is specified what frequencies are going to be tested. Since the resonant frequency is already known, it is not necessary to test the whole spectrum from 0 to 1000 Hz, but it was chosen steps of 100 Hz each, going up and down, the resonant frequency, obtaining 10-15 points for each testing case. The reason for the low number of experimental points was due to a constraint of time, since a lot of other cases also had to be tested. After setting the microphone and created the excel file, $main\_acq.m$ is started. It reads the excel file and stores those values as an array, and commands the signal generator to produce the signals indicated in the file, taking 15 seconds for each frequency step. On conclusion the program stops the signal generator and all files are in a directory provided by the user. Next step is to do the same thing but for the microphone on another location, typically 4 to 5 cm above the neck of the resonator (so that it does not influence the motion of air). This will be the reference signal of the perturbation. Like in the previous case, files for each frequency case are generated in a location provided by the user. The file names are '$Ensaio\_Frequencia\_[a]\_Amp\_[b].csv$' where [a] represents the frequency point and [b] represents the amplitude point.

Next step is to use $main\_proc.m$ to process the raw data and obtain the frequency curves. When running the program for the first time, it prompts the user for 3 directories: two of them being where the files obtained experimentally are located (microphone with probe inside and outside) and one where the results should be located. Then the program proceeds to process the files given and produces a .csv file which possesses the experimental points of interest - frequency, amplitude and phase - as described previously. Then these points are exported to a MATLAB code with the theoretical model to compare it with predictions.

4.3 Samples

4.3.1 Resonator Samples

The five resonators tested were machined in campus at IST. Four resonators were machined from a solid cylinder made out of stainless steel with a polished finish, and another one made with the same process but from aluminum. They were designed so that they follow geometries close to a Helmholtz resonator. Since this work focused on studying small resonators it was decided to (mainly) vary the neck size between them, so it is possible to understand it's influence. Here are all the resonators tested, modeled in SolidWorks:

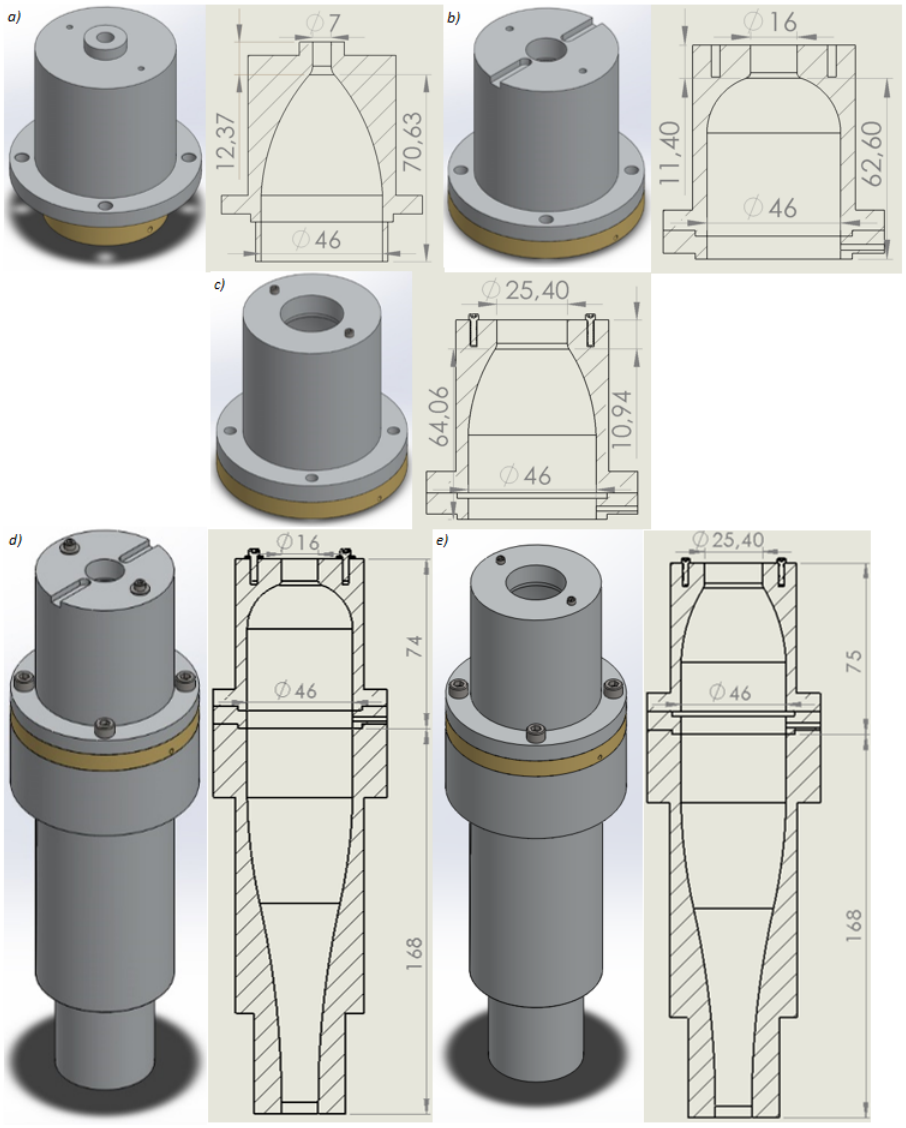

Figure 4.3: a) Resonator 1; b) Resonator 2; c) Resonator 3; d) Resonator 4; e) Resonator 5

4.3.2 Metal Plate Samples

Several metal plates were tested in the facility and are described here. The metal plates are made from stainless steel, the holes are created using laser techniques. The plates have a thickness of $0.5\ mm$ (with exception of plate 4 which has 2 *mm*) and have the same overall size.

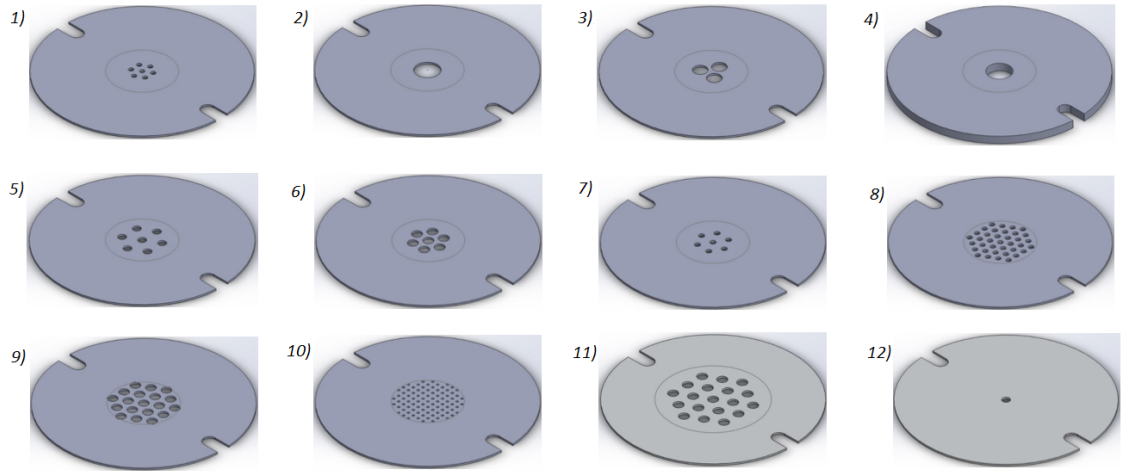

Figure 4.4: 1) Plate 1; 2) Plate 2; 3) Plate 3; 4) Plate 4; 5) Plate 5; 6) Plate 6; 7) Plate 7; 8) Plate 8; 9) Plate 9; 10) Plate 10. 11) Plate 11; 12) Plate 12.

Plate #	n	d_p [mm]	t_p [mm]	dlt [mm]	Perf.Ratio [%]
1	7	1.5	0.5	2.5	43.53
2	1	6	0.5	-	-
3	3	3.5	0.5	5	59.25
4	1	6	2	-	-
5	7	2.5	0.5	4.5	37.32
6	7	2.5	0.5	3.5	61.69
7	7	1.25	0.5	3.5	15.42
8	37	1.5	0.5	2.5	43.53
9	19	2.5	0.5	3.5	61.69
10	85	0.6	0.5	1.5	19.35
11	19	2.5	0.5	4.5	37.32
12	1	1	0.5	-	-

Table 4.1: n = number of holes; d_p = hole diameter; t_p = thickness; dlt = spacing between holes

4.4 Experimental conditions

All acoustic tests were conducted in a large laboratory with ventilation. Temperatures and pressures in the laboratory vary mildly since it is located deep within a building - not subjected to influences from the exterior. However these tests are very sensitive to noise from the background of the lab, since other people and other systems are producing them. Even as much as opening a door which is nearby the installation or people talking can cause disturbances in the signals obtained. Many experiments had to be reevaluated since results did not corroborated with theory due to some of these reasons. All equipment and software provided were in useful condition for these types of experiments.

Chapter 5

Results and discussion

5.1 Helmholtz resonator

The results presented are the amplitude and phase plots for each of the resonators. The theoretical curves plotted in black lines are obtained from the transfer functions, in this case for the Helmholtz resonator given by equation (2.22), and the black squares represent the experimental data for each case. Since the purpose of this work is to model the acoustics of these resonators, the frequency response gives the location of the resonance frequency, which from the thermoacoustics point of view is the instability frequency. The following figures 5.1, 5.2, 5.3, 5.4 and 5.5 show the results for the Helmholtz resonators:

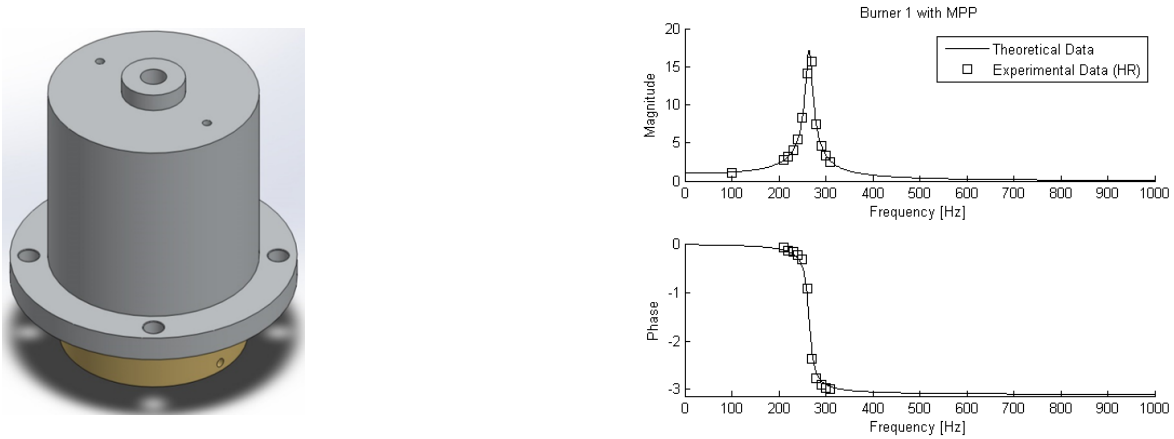

Figure 5.1: Resonator 1; Left: CAD image; Right: Results

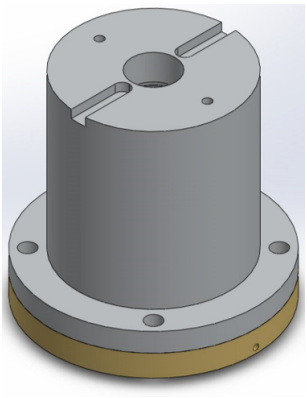

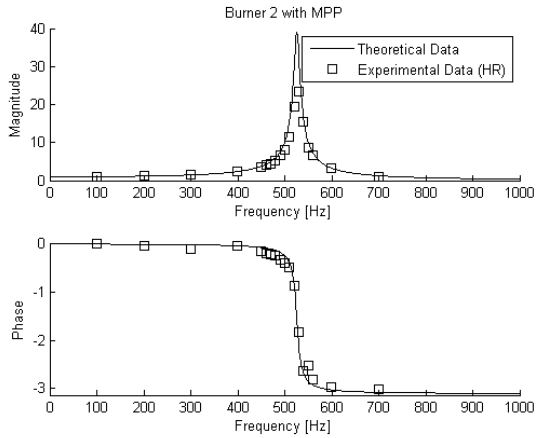

Figure 5.2: Resonator 2; Left: CAD image; Right: Results

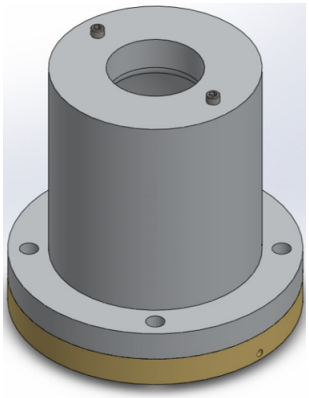

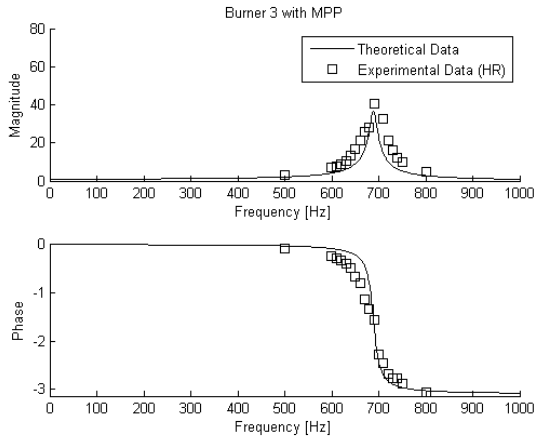

Figure 5.3: Resonator 3; Left: CAD image; Right: Results

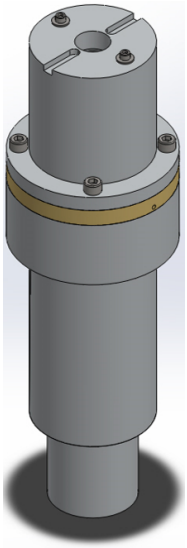

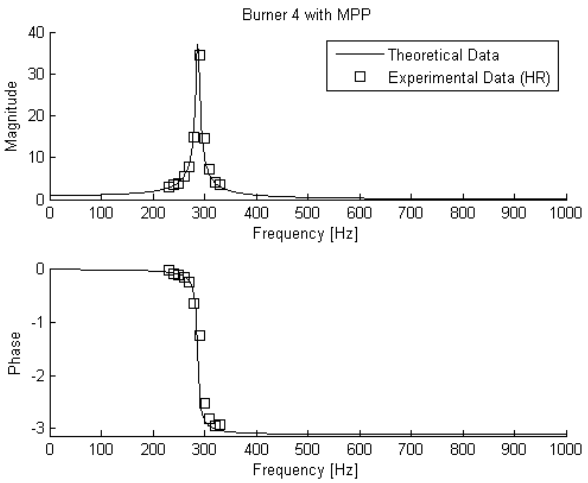

Figure 5.4: Resonator 4; Left: CAD image; Right: Results

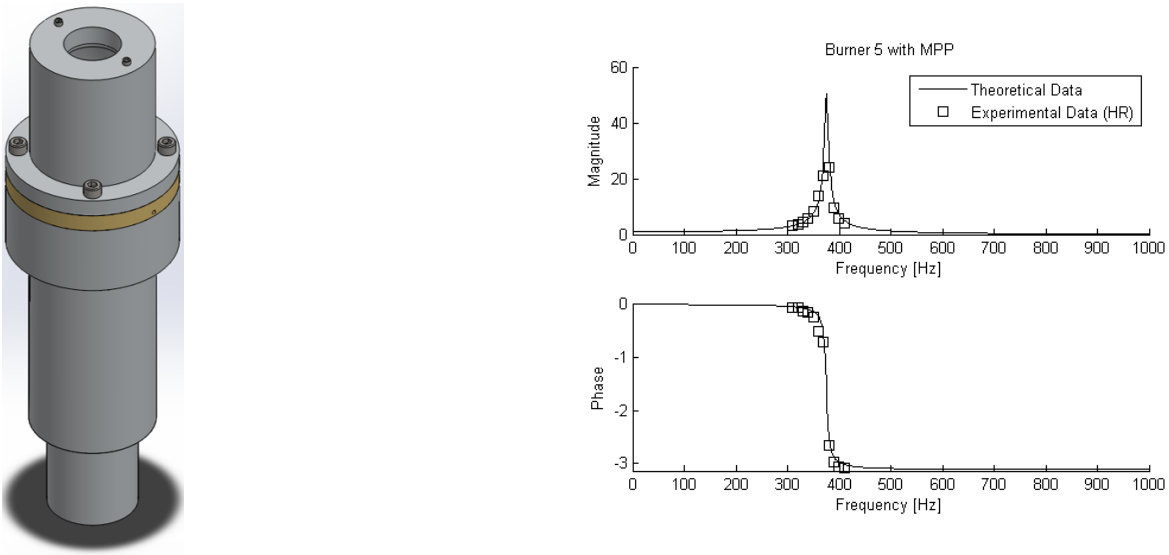

Figure 5.5: Resonator 5; Left: CAD image; Right: Results

Resonator	Resonant frequency [Hz]
1	283
2	523
3	691
4	295
5	379

Table 5.1: Resonator resonant frequencies

The resonance peak is higher with the increase of neck area and is lower with the increase in volume, as expected by looking at the simplified equation (2.24). From these results one can conclude that these resonators follow Helmholtz resonator theory. All results follow very well the theoretical model except for resonator 3 where there is some under damping on the result, even though it was tested several times. This may be due to the fact that this resonator has a very large neck and small cavity unlike the others, which can cause different results since Helmholtz theory starts with the assumption that one is considering a large cavity connected to a small opening. If this condition is not present, the Helmholtz resonator would instead behave as a quarter-wave resonator. Also the losses are very small in these types of resonators, and the maximum difference between the damped and non-damped resonant frequency is about 0.2%.

5.2 Helmholtz resonator with MPP

Following the methodology from the previous section, the transfer function for this case is now equation (3.8) because of the presence of the MPP. It is expected for the resonance frequency to always be lower, independently of the metal plate chosen, since the impedance of the MPP is always positive.

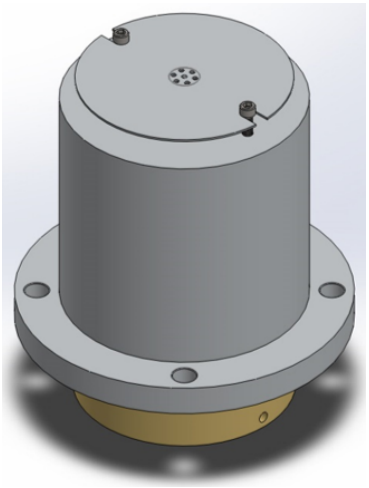

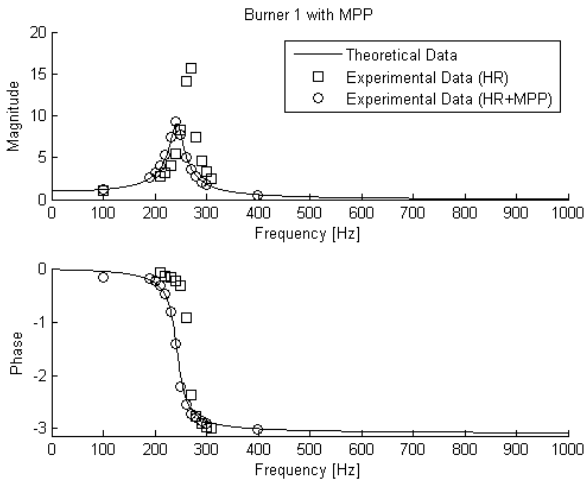

Figure 5.6: Resonator 1 with plate 1; Left: CAD image; Right: Results

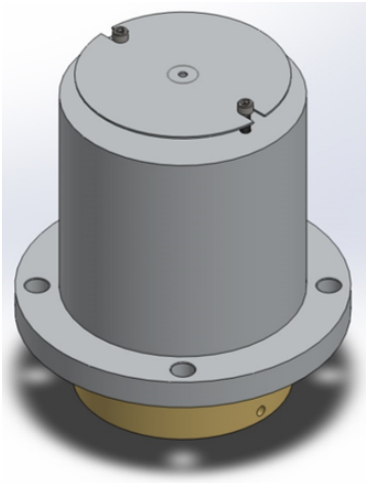

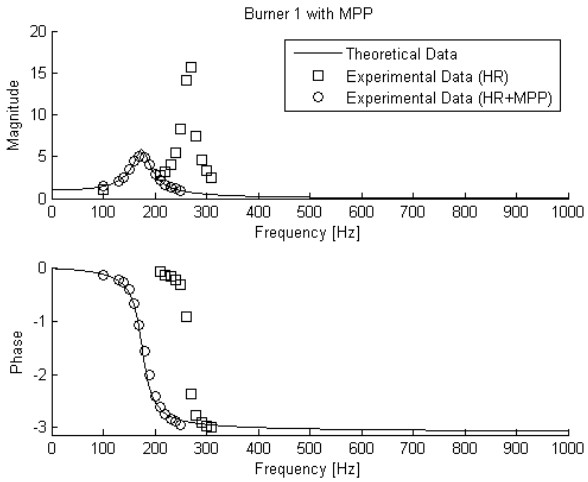

Figure 5.7: Resonator 1 with plate 12; Left: CAD image; Right: Results

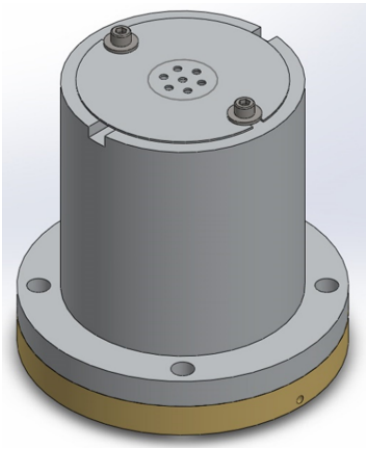

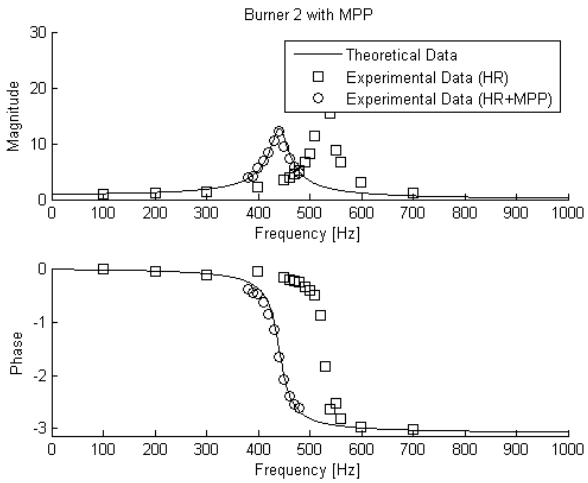

Figure 5.8: Resonator 2 with plate 5; Left: CAD image; Right: Results

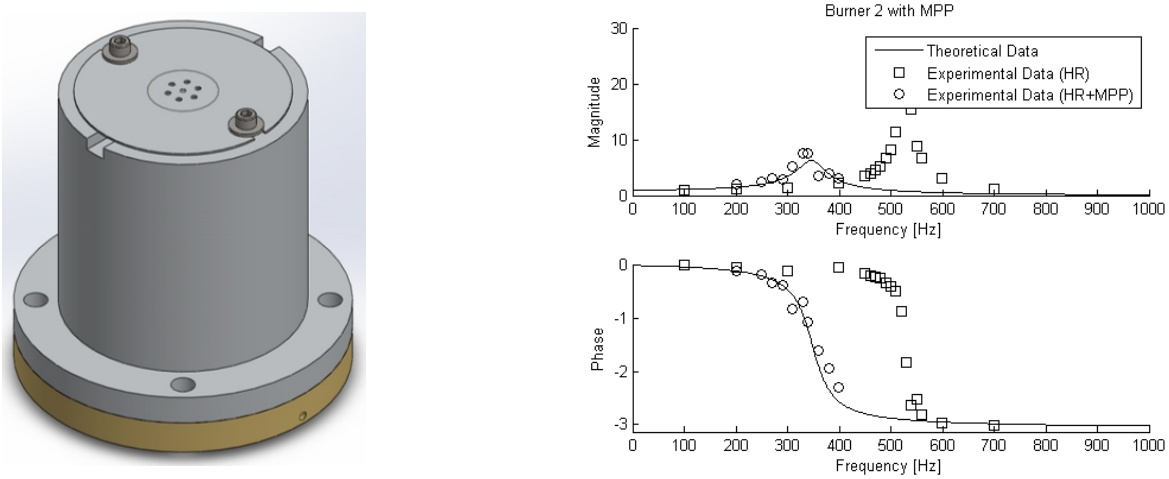

Figure 5.9: Resonator 2 with plate 7; Left: CAD image; Right: Results

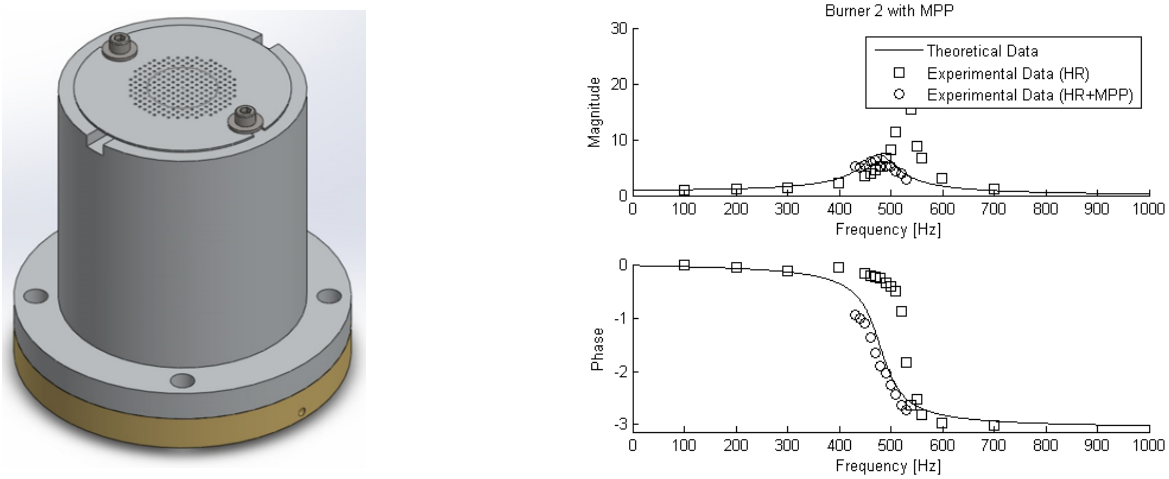

Figure 5.10: Resonator 2 with plate 10; Left: CAD image; Right: Results

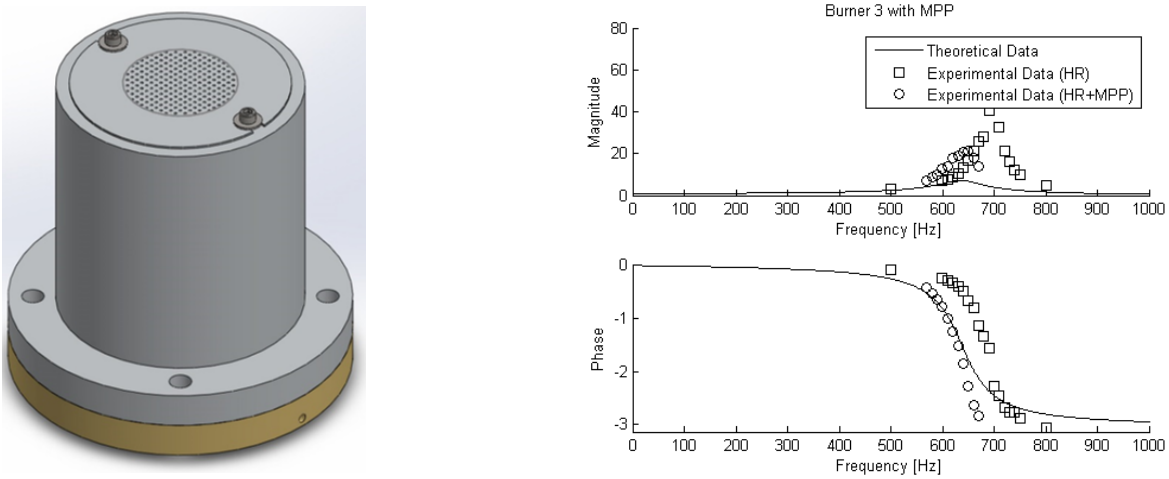

Figure 5.11: Resonator 3 with plate 10; Left: CAD image; Right: Results

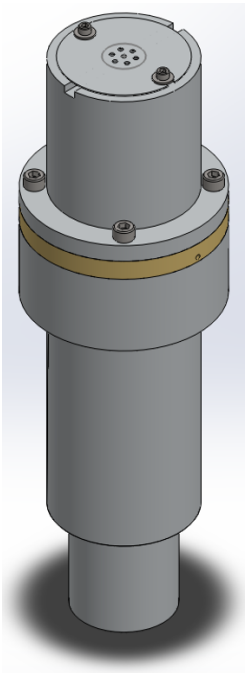

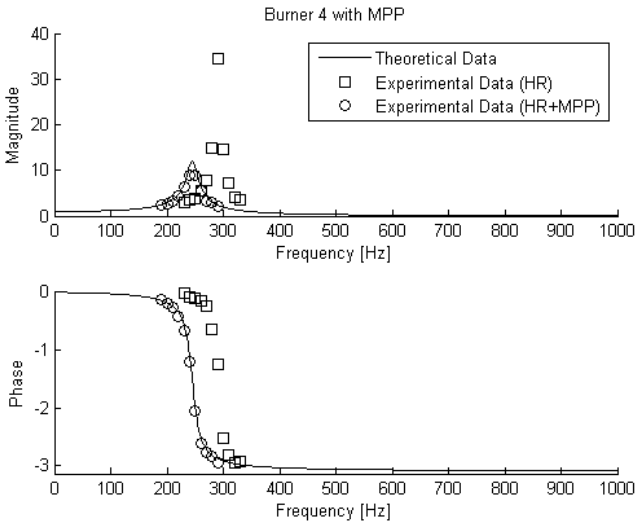

Figure 5.12: Resonator 4 with plate 5; Left: CAD image; Right: Results

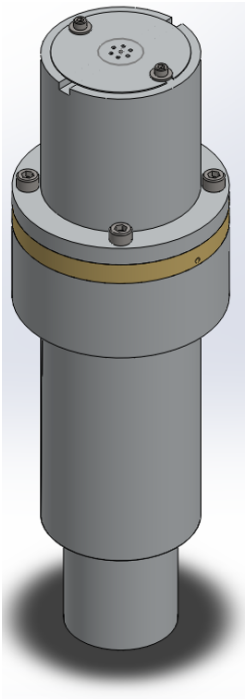

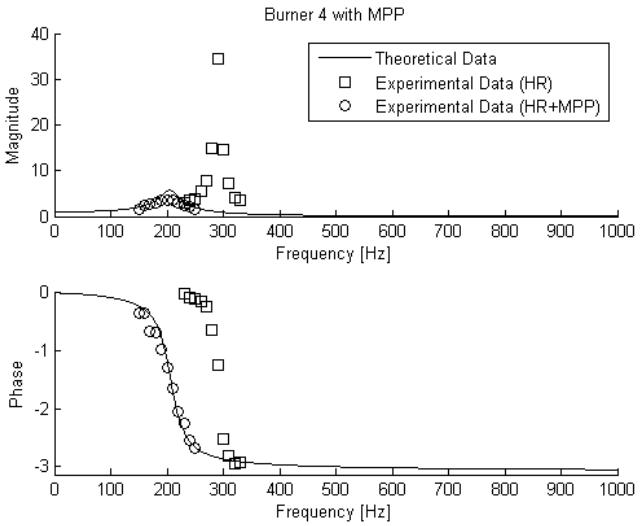

Figure 5.13: Resonator 4 with plate 7; Left: CAD image; Right: Results

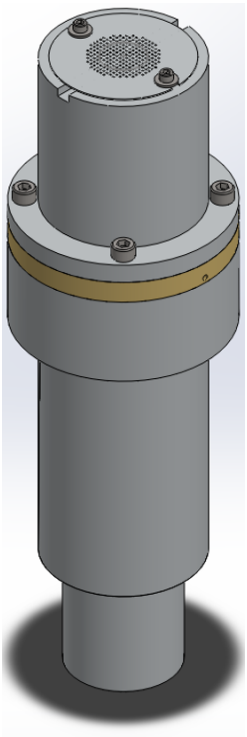

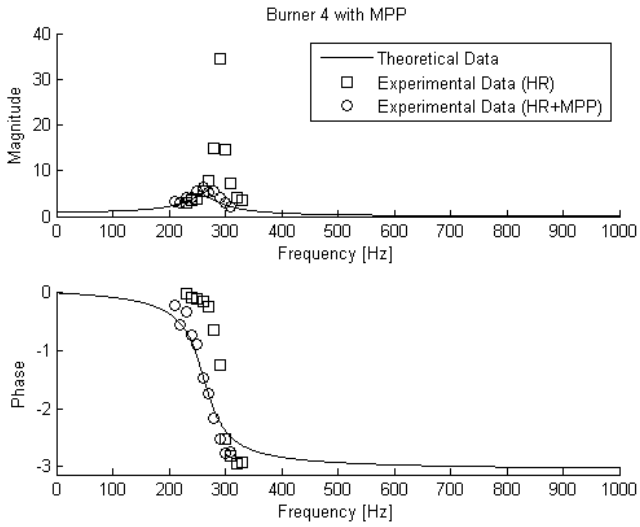

Figure 5.14: Resonator 4 with plate 10; Left: CAD image; Right: Results

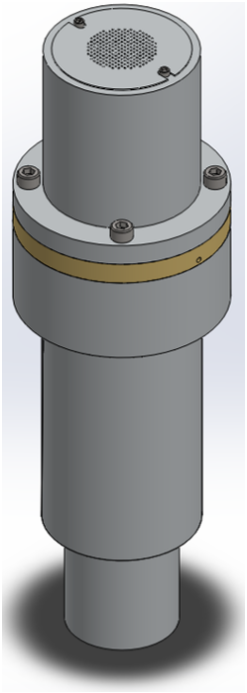

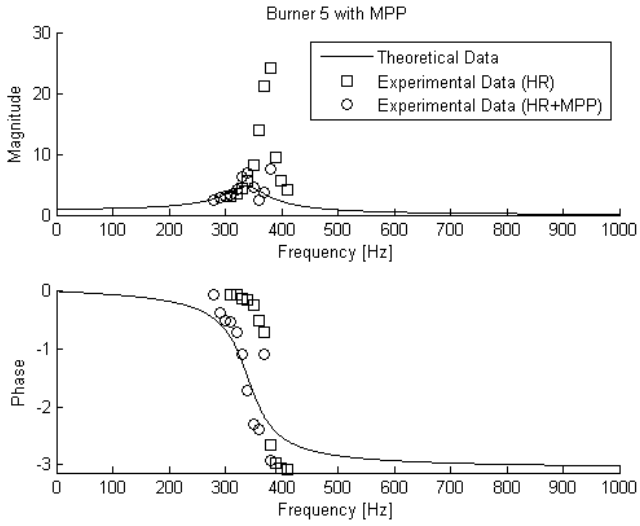

Figure 5.15: Resonator 5 with plate 10; Left: CAD image; Right: Results

Some results show some noise in the signals obtained, probably because as the diameter of the holes decreases further, the pressure fluctuation signals may be harder to obtain inside the cavity. The results show that the theoretical model agrees with the experimental results, except for resonators 3 and 5 (resonator 5 is the same resonator 3 but with the additional coupled volume beneath it), this is probably because this resonator has a large neck compared to the cavity, as explained in the previous

section. For the case of the resonator 1, figure 5.6 shows that introducing the metal plate 1 on top of the neck changes slightly the resonant frequency, unlike placing the metal plate 12 as shown in figure 5.7 where the resonant frequency changes substantially, along with a lower magnitude peak. This suggests that the open area of the MPP - porosity σ - influences greatly the resonant properties of the whole resonator. For resonator 2 one can see the influence of the hole diameter by comparing figures 5.8 and 5.9, where the only difference between them is the hole diameter. As also concluded for resonator 1, by lowering the porosity σ the resonant frequency also lowers. In the case of 5.10 the very large number of holes with very small diameter cause a very high dissipation, hence the very low magnitude peak. For resonator 3 presented in figure 5.11, only metal plate 10 gives good agreement with results, however the theoretical model predicts a larger dissipation then expected since the theoretical curve is below the experimental data. The case of resonator 4 - which is essentially the geometry of resonator 2 coupled with an additional volume (150 ml) below it - shows good results and are presented in figures 5.12 and 5.13. Like in the case of resonator 2, the hole diameter influences substantially the resonant frequency of the system. Finally for resonator 5 - which is resonator 3 with the volume - with plate 10 is plotted on figure 5.15. The results show more noise than in the previous cases, due to the reasons explained on the previous sections. It also should be noted that all resonant frequencies are lower compared to the case without MPP, as expected, along with a lower amplitude peak.

Chapter 6

Conclusions

6.1 Concluding remarks

This study focused on the influence of the introduction of a metal plate on the acoustic properties of the Helmholtz resonator. An extensive research of the Helmholtz resonator was conducted to understand the behavior involved and the mathematical model. Several geometries were used in order to understand the influence of neck and the volume on acoustics of the resonator. The diameter of the necks ranged from $7 - 25.4$ mm, and the volume of the cavity of the resonators ranged from $90 - 250 * 10^{-6}$ m^3. An experimental installation was developed to test the resonators, which were tested by obtaining two time signals from a microphone - caused by a speaker that was mounted on the installation - one obtained inside the resonator cavity and one outside as a reference signal. The reference frequency range for was between $1 - 1000$ Hz. After these signals were obtained, they were processed using FFT (Fast Fourier Transform) method to produce magnitude and phase data, which will be compared with the theoretical results given by the transfer function. The theoretical results for the Helmholtz resonator without MPP show very good agreement with experiments. Then the metal plate was introduced on top of the resonator to study the impact on resonant frequency, which was the original objective of this work. The plates have a thickness of 0.5 mm with varying geometry configurations for the perforated holes, with hole diameters ranging from $0.6 - 6$ mm and hole spacing from $1.5 - 5$ mm. The mathematical model combines two models from different authors to simulate the whole resonator. The experimental results for the resonator with the MPP also show very good agreement with the theoretical model, and they were obtained using the same method for the previous case. It was observed that the resonance frequency, when the MPP is introduced in the Helmholtz resonator, is lowered according to the characteristics of the metal plate, such as the porosity and perforation ratio.

6.2 Future work

The next step would be to extend the model to be able to simulate metal plates beyond the theory restrictions, by using for instance empirical correlations applied to the end-corrections factors for plates

with large porosity or very small perforation ratios (for example). Since such cases can be found in practical application the development of the current work is necessary to adjust for these applications.

Bibliography

[1] A. Selamet, V. Kothamasu, and J. Novak, “Insertion loss of a helmholtz resonator in the intake system of internal combustion engines: an experimental and computational investigation,” *Applied Acoustics*, vol. 62, no. 4, pp. 381 – 409, 2001.

[2] B. Cintra and E. Fernandes, “Thermoacoustic instabilities of lean disc flames,” *Fuel*, vol. 184, pp. 973 – 986, 2016.

[3] M. Alster, “Improved calculation of resonant frequencies of helmholtz resonators,” *Journal of Sound and Vibration*, vol. 24, no. 1, pp. 63 – 85, 1972.

[4] U. Ingard, “On the theory and design of acoustic resonators,” *The Journal of the acoustical society of America*, vol. 25, no. 6, pp. 1037–1061, 1953.

[5] L. Kinsler, *Fundamentals of acoustics*. Wiley, 2000.

[6] M. L. Munjal, *Acoustics of ducts and mufflers with application to exhaust and ventilation system design*. John Wiley & Sons, 1987.

[7] N. Dickey and A. Selamet, “Helmholtz resonators: one-dimensional limit for small cavity length-to-diameter ratios,” *Journal of Sound and Vibration*, vol. 195, no. 3, pp. 512–517, 1996.

[8] R. L. Panton and J. M. Miller, “Resonant frequencies of cylindrical helmholtz resonators,” *The Journal of the Acoustical Society of America*, vol. 57, no. 6, pp. 1533–1535, 1975.

[9] A. Selamet, N. Dickey, P. Radavich, and J. Novak, “Theoretical, computational and experimental investigation of helmholtz resonators: one-dimensional versus multi-dimensional approach,” SAE Technical Paper, Tech. Rep., 1994.

[10] A. Selamet, P. Radavich, N. Dickey, and J. Novak, “Circular concentric helmholtz resonators,” *The Journal of the Acoustical Society of America*, vol. 101, no. 1, pp. 41–51, 1997.

[11] A. Selamet and Z. Ji, “Circular asymmetric helmholtz resonators,” *The Journal of the Acoustical Society of America*, vol. 107, no. 5, pp. 2360–2369, 2000.

[12] A. Selamet and I. Lee, “Helmholtz resonator with extended neck,” *the Journal of the Acoustical Society of America*, vol. 113, no. 4, pp. 1975–1985, 2003.

[13] A. Selamet, M. Xu, I.-J. Lee, and N. Huff, “Helmholtz resonator lined with absorbing material,” *The Journal of the Acoustical Society of America*, vol. 117, no. 2, pp. 725–733, 2005.

[14] S. Tang, “On helmholtz resonators with tapered necks,” *Journal of Sound and Vibration*, vol. 279, no. 3, pp. 1085 – 1096, 2005.

[15] D. Wan and D. T. Soedel, “Two degree of freedom helmholtz resonator analysis,” SAE Technical Paper, Tech. Rep., 2004.

[16] J. M. De Bedout, “Adaptive-passive noise control with self-tuning helmholtz resonators,” Ph.D. dissertation, Citeseer, 1996.

[17] S. Griffin, S. A. Lane, and S. Huybrechts, “Coupled helmholtz resonators for acoustic attenuation,” *Journal of vibration and acoustics*, vol. 123, no. 1, pp. 11–17, 2001.

[18] U. Ingard and H. Ising, “Acoustic nonlinearity of an orifice,” *The journal of the Acoustical Society of America*, vol. 42, no. 1, pp. 6–17, 1967.

[19] M. A. Temiz, J. Tournadre, I. L. Arteaga, and A. Hirschberg, “Non-linear acoustic transfer impedance of micro-perforated plates with circular orifices,” *Journal of Sound and Vibration*, vol. 366, pp. 418 – 428, 2016.

[20] J.-M. Roche, L. Leylekian, and F. Vuillot, “Acoustic and aerodynamic dissipations induced by a sound wave-impacted helmholtz resonator,” *Journal of the Acoustical Society of America*, vol. 123, no. 5, p. 3250, 2008.

[21] N. Dickey and A. Selamet, “Helmholtz resonators: One-dimensional limit for small cavity length-to-diameter ratios,” *Journal of Sound and Vibration*, vol. 195, no. 3, pp. 512 – 517, 1996.

[22] S. Horowitz, T. Nishida, L. Cattafesta, and M. Sheplak, “Characterization of compliant-backplate helmholtz resonators for an electromechanical acoustic liner,” *International Journal of Aeroacoustics*, vol. 1, no. 2, pp. 183–205, APR 2002.

[23] X. Shi and C. M. Mak, “Helmholtz resonator with a spiral neck,” *Applied Acoustics*, vol. 99, pp. 68 – 71, 2015.

[24] M. Xu, A. Selamet, and H. Kim, “Dual helmholtz resonator,” *Applied Acoustics*, vol. 71, no. 9, pp. 822 – 829, 2010.

[25] A. Suzuki, H. Takahashi, E. Iwase, K. Matsumoto, and I. Shimoyama, “Sensitivity enhancement by micro helmholtz resonator for ultrasonic distance sensor,” in *Solid-State Sensors, Actuators and Microsystems Conference, 2009. TRANSDUCERS 2009. International*, June 2009, pp. 1557–1560.

[26] S. Konishi, M. Yoda, S. Sugiyama, and S. Akishita, “Tunable acoustic absorber using a micro acoustic hole array,” *Electronics and Communications in Japan (Part II: Electronics)*, vol. 83, no. 1, pp. 1–6, 2000.

[27] D.-Y. Maa, “Potential of microperforated panel absorber,” *the Journal of the Acoustical Society of America*, vol. 104, no. 5, pp. 2861–2866, 1998.